Available online at www.sciencedirect.com

ScienceDirect

Geochimica et Cosmochimica Acta 285 (2020) 129–149

Geochimica et Cosmochimica Acta

www.elsevier.com/locate/gca

Heterogeneous nickel isotopic compositions in the terrestrial mantle – Part 1: Ultramafic lithologies

Naomi J. Saunders [a,b,*], Jane Barling [a], Jason Harvey [c], Alex N. Halliday [a,b]

[a] Dept of Earth Sciences, University of Oxford, South Parks Road, Oxford OX1 3AN, UK
[b] Lamont-Doherty Earth Observatory, Columbia University, 61 Route 9W, Palisades 10964, USA
[c] School of Earth and Environment, University of Leeds, Leeds LS2 9JT, UK

Received 15 October 2019; accepted in revised form 18 June 2020; Available online 3 July 2020

Abstract

High precision nickel stable isotopic compositions ($\delta^{60/58}$Ni) are reported for 22 peridotite xenoliths from the USA (Kilbourne Hole, New Mexico), Tanzania, and Cameroon. For a subset of these, $\delta^{60/58}$Ni is also reported for their constituent mineral separates (olivine, orthopyroxene, clinopyroxene, and spinel). Bulk peridotites show significant heterogeneity in Ni isotopic composition, ranging from +0.02‰ to +0.26‰. Unmetasomatised fertile peridotites from three localities, define an average $\delta^{60/58}$Ni of +0.19±0.09‰ (n = 18). This value is comparable to previous estimates for the $\delta^{60/58}$Ni of the bulk silicate earth (BSE), but is unlikely to be representative, given observed heterogeneity, presented here and elsewhere. Samples with reaction rims and interstitial glass (interpreted as petrographic indications of minor metasomatism) were excluded from this average; their Ni isotopic compositions extend to lighter values, spanning nearly the entire range observed in peridotite worldwide. Dunites (n = 2) are lighter in $\delta^{60/58}$Ni than lherzolites and harzburgites from the same location, and pyroxenites (n = 5) range from +0.16‰ to as light as −0.38‰.

The $\delta^{60/58}$Ni in the Kilbourne Hole xenoliths correlate negatively with bulk-rock Fe concentration and positively with ^{143}Nd/^{144}Nd, providing evidence that light $\delta^{60/58}$Ni is associated with mantle fertility and enrichment. The trend between $\delta^{60/58}$Ni and Fe concentration in bulk rocks appears to be global, replicated across the peridotites in this work from other localities, and in literature data.

The inter-mineral fractionations are small; the maximum difference between heaviest and lightest phase is 0.12‰. This provides evidence that bulk rock $\delta^{60/58}$Ni variation does not result from differences in modal mineralogy, fractional crystallization or degrees of partial melting. The $\delta^{60/58}$Ni fractionation appears to be an equilibrium effect and usually is in the decreasing order spinel > olivine = orthopyroxene > clinopyroxene. However, the fractionation between clinopyroxene and orthopyroxene varies in magnitude and sign, and is correlated with pyroxene Si/Fe positively, and Fe/Mg negatively. The magnitude of inter-pyroxene fractionation also correlates with other pyroxene compositional ratios (e.g. $La/Sm_{clinopyroxene}$); as well as bulk rock $\delta^{60/58}$Ni, and [U]. These data provide evidence that Ni isotopes fractionate at the bulk rock and mineral scale in response to mantle enrichment processes, possibly related to recycling of isotopically light subducted components.

Keywords: Non-traditional isotope systems; Nickel; Mantle; Recycling; Peridotites; Pyroxenites

1. INTRODUCTION

Nickel (Ni) is a first row transition metal with five stable isotopes whose relative abundances vary widely: ^{58}Ni (68.08%), ^{60}Ni (26.22%), ^{61}Ni (1.11%), ^{62}Ni

* Corresponding author.
E-mail address: naomi.saunders@mail.com (N.J. Saunders).

https://doi.org/10.1016/j.gca.2020.06.029
0016-7037/

(3.64%), and ^{64}Ni (0.93%) (Gramlich et al., 2012). An estimated 99.97% of the Ni budget of the bulk silicate Earth (BSE) resides in the mantle (McDonough and Sun, 1995). In natural terrestrial environments Ni is almost exclusively in the 2^+ valence state (Nicholls, 1974). Therefore, Ni provides an opportunity to investigate high temperature processes without the effects of changing oxidation state, which can affect other isotopic systems. Nickel has a similar ionic radius and charge to magnesium; therefore, the Ni^{2+} ion partitions readily into the octahedral metal sites in olivine and pyroxenes (Burns, 1970), leading to rapid decrease in Ni concentrations during magmatic differentiation of Mg-rich minerals. Nickel, as a compatible element, will be less sensitive to mantle processes than signatures which can be perturbed by melting processes, such as melting and metasomatism whose influences are more clearly seen in the systematics of more incompatible trace elements.

Published stable Ni isotope compositions ($\delta^{60/58}$Ni, defined as the ratio of isotope 60 to 58, relative to the same in SRM986, expressed in per mille) of terrestrial materials are presented in Fig. 1. The majority of mantle $\delta^{60/58}$Ni data has been published within the last 4 years (Gall et al., 2017; Klaver et al., 2020). The data for ultramafic xenoliths show a range in $\delta^{60/58}$Ni = +0.04‰ to +0.36‰ (Ratié et al., 2015; Gall et al., 2017; Spivak-Birndorf et al., 2018; Klaver et al., 2020). Ultramafic rock standards, analysed for inter-laboratory comparison, range from −0.08‰ (DTS1) through JP1 and DTS2 to +0.34‰ for PCC1 (although later analyses of PCC1 average +0.14‰), (Cameron et al., 2009; Gall, 2011; Steele et al., 2011, 2012; Gall et al., 2012, 2017; Gueguen et al., 2013; Chernonozhkin et al., 2015; Klaver et al., 2020).

A reported relationship between ultramafic xenolith Ni isotopic compositions and modal mineralogy, specifically clinopyroxene content (Gall et al., 2017) is not supported by the most recent data (Klaver et al., 2020). Komatiites, which are products of large degree partial melting of the mantle, have been shown to have similar Ni isotopic compositions to ultramafic xenoliths. This has provided evidence that residual olivine does not significantly fractionate Ni isotopic compositions (Gall et al., 2017). Similarly, no correlations were found between $\delta^{60/58}$Ni in ultramafic xenoliths and bulk rock Al_2O_3, inferred to show no control on Ni isotopic composition with geochemical indices of depletion (Klaver et al., 2020).

Archean komatiites with disseminated sulphide have more variable $\delta^{60/58}$Ni, lighter than Tertiary komatiites (Gall, 2011; Gueguen et al., 2013). Sulphide minerals have shown wide ranging $\delta^{60/58}$Ni from −1.05‰ to +0.76‰ (Tanimizu and Hirata, 2006; Gall, 2011; Gueguen et al., 2013; Hofmann et al., 2014), and this is also true for specific sulphide mineral species. For example, samples of pentlandite range from −1.05‰ (Tanimizu and Hirata, 2006) to +0.58‰ (Gall, 2011). Sulphide metasomatism has been proposed to explain lighter Ni isotopic compositions in a minority of peridotite xenoliths (Klaver et al., 2020). In the same work, combinations of silicate and carbonatitic metasomatism were proposed to produce heavier Ni isotopic compositions (Klaver et al., 2020).

Nickel isotopic compositions for (ultra-)mafic minerals are limited to 6 peridotite-hosted olivine separates (+0.04‰ to +0.16‰, (Spivak-Birndorf et al., 2018; Klaver et al., 2020); and 5 peridotite-hosted mineral separates (Gall et al. 2017) from 3 peridotite xenoliths: olivine (+0.14‰, +0.17‰); orthopyroxene (−0.04‰, −0.02‰); and clinopyroxene (+2.89‰). Additionally, basalt-hosted olivine has been found to fall within the range observed for peridotite-hosted olivine (+0.10‰; Gueguen et al., 2013). Minimal fractionations have been observed between the composition of the olivine separate and its respective host. Five olivine-host pairs analysed by Klaver et al. (2020) showed differences in Ni isotopic composition less than +0.06‰. Megacrysts (Gall et al., 2017) are not considered in this work, as their relationship to mantle rocks is unknown.

Estimates for the BSE range from +0.11‰ (Elliott and Steele, 2017) to +0.23‰ (Gall et al., 2017), with the most recent estimate +0.12‰ (Klaver et al., 2020) supporting a lighter composition. However, with the observed range in Ni isotopic compositions of ultramafic xenoliths (−0.08‰ to +0.36‰), it is uncertain how much a single average can represent the Ni isotopic composition of the silicate Earth. Here we explore the causes for this apparent variability with more detailed studies of ultramafic rocks including constituent minerals.

2. TECTONIC SETTING AND SAMPLE DESCRIPTIONS

Ultramafic xenoliths selected for this study came from New Mexico, USA (n = 18), Tanzania (n = 7), and Cameroon (n = 5). Xenoliths with metasomatic phases were excluded, as were xenoliths with evidence of significant alteration (for example: weathering, oxidation, serpentinization), in order eliminate any effect from such fluid-related processes. Chondrite normalised incompatible element and selected major elements plots are provided in the supplementary information for further characterisation of the samples (Electronic Annex Figs. A1 and A2). Selected major and trace element data is presented in Tables A1 and A2.

2.1. Kilbourne Hole, New Mexico, USA

Kilbourne Hole (31°59′N, 106°57′W) is a volcanic maar to the east of the Late Pleistocene Potrillo Volcanic Field, located near the axis of the Rio Grande Rift. The xenoliths are hosted in a basanite lava. The xenoliths at this locality include a range of dominantly protogranular anhydrous spinel lherzolites and spinel harzburgites. Pyroxenite xenoliths are also present, as a subsidiary lithology, observed as typically decimetre-sized layers with sharp mineralogical boundaries in the host peridotite (Irving, 1980). The relatively young age of the basanite that brought the ultramafic xenoliths to the surface, ~10 Ka; (Satsukawa et al., 2011), suggests that these peridotite xenoliths are representative of the modern day sub-continental lithospheric mantle beneath Kilbourne Hole. Harvey et al. (2012) calculated equilibrium temperatures between 989 and 1181°C for

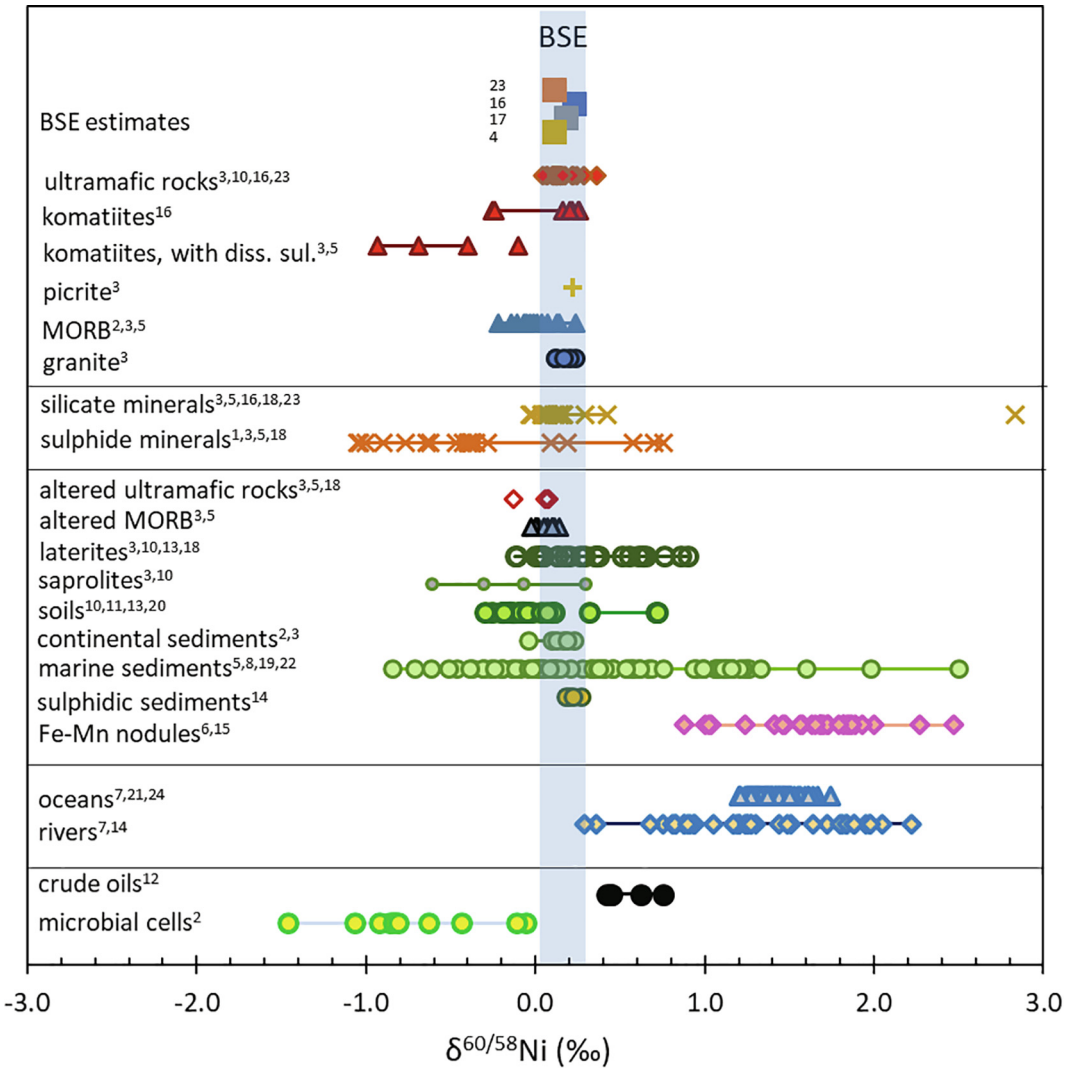

Fig. 1. Published $\delta^{60/58}$Ni data for terrestrial samples, excluding reference materials. BSE estimates for comparison, from Steele et al. (2011), Gall et al. (2017), Klaver et al. (2020) and with the estimate of Gueguen et al. (2013) recalculated by Elliott and Steele (2017) to remove sediments. [1]Tanimizu and Hirata, 2006; [2]Cameron et al., 2009; [3]Gall, 2011; [4]Steele et al., 2011; [5]Gueguen et al., 2013; [6]Gall et al., 2013; [7]Cameron and Vance, 2014; [8]Porter et al., 2014; [9]Hofmann et al., 2014; [10]Ratié et al., 2015; [11]Estrade et al., 2015; [12]Ventura et al., 2015; [13]Ratié et al., 2016; [14]Vance et al., 2016; [15]Gueguen et al., 2016; [16]Gall et al., 2017; [17]Elliott and Steele, 2017; [18]Spivak-Birndorf et al., 2018; [19]Ciscato et al., 2018; [20]Ratié et al., 2019; [21]Wang et al., 2019; [22]Pašava et al., 2019; [23]Klaver et al., 2020; [24] Archer et al., 2020.

Kilbourne Hole xenoliths, using the method of Brey and Köhler (1990). Protogranular peridotite xenoliths from Kilbourne Hole are inferred to have last equilibrated at >1.8 GPa (Kil and Wendlandt, 2007).

Modal mineral abundances, and major and trace element data for both bulk-peridotites and minerals demonstrate that Kilbourne Hole peridotites have experienced less than 20% melt depletion (Perkins and Anthony, 2011; Harvey et al., 2012). Further, the preservation of Re-Os isotope evidence for ancient melt depletion events in some Kilbourne Hole xenoliths (Harvey et al., 2011), suggests that elements compatible during partial melting, such as Os and Ni, have been largely undisturbed by metasomatism subsequent to melt-depletion. The pyroxenite-forming event at Kilbourne Hole has been associated with the infiltration and equilibration of a primitive basanite magma with lherzolite wall-rocks (Roden et al., 1988), resulting in incompatible element enrichment in the neighbouring wall-rock (Roden et al., 1988).

Subsequent to varying degrees of melt depletion, the Kilbourne Hole peridotites have experienced variable, generally minor, melt-rock interaction/refertilization, and cryptic metasomatic events (Kil and Wendlandt, 2007; Harvey et al., 2012). Kil and Wendlandt (2007) proposed 2 discrete metasomatic events affecting Kilbourne Hole: the first prior to rifting and related to subduction of the Farallon plate (140–37 Ma), and one more recently involving infiltration of the basanite in which the xenoliths were brought to the surface. No examples of discrete metasomatic phases or serpentinization have been

found in Kilbourne Hole xenoliths (Harvey et al., 2012, 2015).

Peridotite xenolith LREE/HREE ratios have been used to identify samples that have undergone melt extraction without significant subsequent metasomatism (Wilshire, 1984; Kil and Wendlandt, 2007). Harvey et al. (2015) used $(La/Yb)_N$ (where N refers to normalisation to Primitive Mantle; McDonough and Sun, 1995) to broadly segregate Kilbourne Hole peridotites into two groups, $(La/Yb)_N < 1$ and $(La/Yb)_N > 1$ (Harvey et al., 2015). The xenoliths exhibit a continuum in $(La/Yb)_N$, and the cut-off value of 1 is arbitrary; chosen to distinguish between samples where incompatible trace elements must have been perturbed by metasomatism ($(La/Yb)_N > 1$) and those samples which only may have experienced little or no perturbation to their incompatible trace elements ($(La/Yb)_N < 1$).

The petrology and composition of the peridotites studied here are a subset from those previously characterised by Harvey et al. (2012). These samples were chosen to include harzbugitic, lherzolitic, and pyroxenitic lithologies. The majority of the samples are unmetasomatised, but the suite does include 6 peridotite xenoliths displaying evidence of small degrees of metasomatism (Harvey et al., 2012). This is evidenced by interstitial glass (KH03-15, KH03-16, KH03-21) and clinopyroxene reaction rims (KH03-10, KH03-15, KH03-24, KH03-27), both of which are inferred to have been produced by a single metasomatic event (Harvey et al., 2012). The major phases in the Kilbourne Hole pyroxenites studied here are clinopyroxenes, with olivine as a minor phase. The clinopyroxene that dominates these pyroxenites are dominantly Al-augite, rather than the Cr-diopside that dominates the peridotites from this location. Quantative modal mineralogy has not been determined for the pyroxenites.

2.2. Lashaine and Labait Hill, Tanzania

The two Tanzanian localities, Lashaine (3°22′S, 36°26′E) and Labait Hill (4°34′S, 35°26′E), are volcanoes on the eastern branch of the East African Rift. The lithosphere is thicker beneath the eastern margin of that branch nearer Lashaine, than the western margin near Labait Hill (Gibson et al., 2013). In general, Tanzanian xenoliths are subject to highly variable degrees and styles of metasomatism (Gibson et al., 2013).

2.2.1. Lashaine

Lashaine is an ankaramitic and carbonatitic tuff cone ~90 km SE of Oldoinyo Loolmurwak, on the Monduli plains. Xenoliths from Lashaine are not genetically linked to the ankaramite host lavas (Rhodes and Dawson, 1975; Ridley and Dawson, 1975). Xenoliths are dominantly garnet-free peridotites (Dawson et al., 1970; Pike et al., 1980) and spinel is present as a minor phase in about half of the peridotites studied in Reid et al. (1975). Pyroxenite xenoliths are also present at Lashaine (Dawson and Smith, 1973; Pike et al., 1980). The temperature and pressure of the last equilibration of garnet-bearing xenoliths was estimated at 960–1085°C and 3.2–5.0 GPa (Gibson et al., 2013) using the methods of Brey and Köhler (1990) and Brey et al. (1990). The temperatures obtained for garnet-bearing peridotites have been assumed to also apply to garnet-free peridotites, based on their otherwise similar mineral compositions (Reid et al., 1975).

Peridotite xenoliths from Lashaine are the product of less than 35% melt depletion, assuming MgO and SiO_2 have not been significantly altered by metasomatism (Gibson et al., 2013). The melt depletion event is dated at ~3.4 Ga, from Re-Os model ages (Burton et al., 2000) and produced a high-olivine restite. The restite experienced two episodes of metasomatism (Dawson, 2002; Gibson et al., 2013). Lashaine xenoliths have shown extremely variable isotopic compositions in Nd, Sr, and Pb, (e.g. Cohen et al., 1984). These isotopic compositions have been related to metasomatism and/or influence from recycled material (Cohen et al., 1984). No evidence of inter-mineral disequilibrium is observed in samples without clinopyroxene breakdown or interstitial glass (Reid et al., 1975). Little to no evidence of near-surface alteration or contamination during transport has been observed (Reid et al., 1975; Rhodes and Dawson, 1975) and no evidence of significant hydrothermal alteration is observed (Gibson et al., 2013). The olivines in the xenoliths used here have been described as unserpentinised and fresh (Reid and Dawson, 1972).

The peridotites analysed here from Lashaine show no evidence of contamination during transport or subsequently (Rhodes and Dawson, 1975). They have unaltered olivines (Reid and Dawson, 1972). The mineral proportions range from 84 to 90% olivine, with 4–12% orthopyroxene and minor chromite (Reid et al., 1975). Clinopyroxene was not observed in the samples, but inclusion of clinpyroxene provides a better fit to the bulk rock composition (Reid et al., 1975). Two dunite samples were analysed from this locality. It is likely that some alteration has affected these samples (e.g. Dawson, 2002). Dunite, BD806, has been described as having more elevated K_2O, TiO_2, and both ferric and ferrous iron, compared with the peridotites at the same site (Dawson et al., 1970). Modal mineralogy of this sample has not been published. Dunite, BD825, has also been described as iron rich (Rhodes and Dawson, 1975). This xenolith is 92.7% olivine, with clinopyroxene (2.2%) and chromite (0.7%) as minor phases, calculated from least squares regression based on microprobe data (Rhodes and Dawson, 1975).

The dunites sampled from Lasahine were chosen to complement the Kilbourne Hole xenolith suite, as that lithology is absent at Kilbourne Hole. The spinel lherzolites analysed here were chosen for comparison with Kilbourne Hole samples of the same lithology.

2.2.2. Labait Hill

Labait Hill is a small volcano, 150 km SW of Lashaine, located on a suture zone between the Archean Tanzanian craton and the Proterozoic Mozambique mobile belt. The volcano is dominated by melilitic lavas, and is of Quaternary age (Lee and Rudnick, 1999a; Dawson, 2012). Labait

Hill xenoliths are therefore likely to sample present-day Tanzanian sub-continental lithospheric mantle. Labait Hill xenoliths comprise dominantly Fe-rich dunites, with less than 10% garnet or spinel-bearing harzburgites and lherzolites (Koornneef et al., 2009). Minor pyroxenites and glimmerites also occur (Koornneef et al., 2009). These can be variably altered. Equilibration temperatures for xenoliths from this locality range from 925 to 1406°C (Paslick, 1995; Lee and Rudnick, 1999a; Zhang et al., 2018), using 2 pyroxene geothermometers (Brey and Köhler, 1990). Pressures calculated by Paslick (1995) for the garnet lherzolites correspond to 110–140 km using Brey and Köhler (1990). Pressure data for garnet-free lithologies is not available.

Xenoliths from this locality preserve evidence of a depletion event followed by a cryptic metasomatic overprint (Dawson, 1999). Different generations of secondary mineral phases observed in some Labait Hill xenoliths are observed in variable states of equilibration (Koornneef et al., 2009). The most pervasive metasomatic event at Labait Hill has been proposed to be related to the Pan African Orogeny, which could cause the introduction or re-activation of fluids in the lithospheric mantle (Koornneef et al., 2009). All olivine in Labait Hill xenoliths is unzoned (Paslick, 1995; Lee and Rudnick, 1999b). Labait Hill garnet peridotites have very high $^{238}U/^{204}Pb$ (e.g. H93-X1 = 618, H93-X9 = 1452), which has been suggested to indicate a very recent metasomatic event (Paslick, 1995), as the Pb isotopic composition is insufficiently radiogenic ($^{206}Pb/^{204}Pb < 18$) for significant decay of ^{238}U (Paslick, 1995). Peridotite xenoliths also have relatively enriched Nd isotopic compositions (e.g. H93-X1 $\varepsilon Nd = -6.8$ and H93-X9 $\varepsilon Nd = 0.8$). Further information on the metasomatic history of this locality, as exhibited in xenoliths that were not used in this work, may be found in the Electronic Appendix.

Three Labait Hill xenoliths are analysed in this work: two garnet-bearing lherzolites (H93-X1 and H93-X9); and one spinel-bearing lherzolite (H93-X8). Garnet in both garnet lherzolites has reacted to form spinel-orthopyroxene-diopside intergrowths and only relict cores of garnet remain (Paslick, 1995). H93-X1 is known to have a equigranular texture (Paslick, 1995), but textural information for other xenoliths is unknown. The samples for this work were chosen to avoid any xenoliths with metasomatic phases, although H93-X8 and H93-X9 have been decribed as altered more extensively than other xenoltihs from this locality (Paslick, 1995).

The garnet lherzolites sampled here were chosen to complement the Kilbourne Hole xenolith suite, as that lithology is absent at Kilbourne Hole. The spinel lherzolite was chosen for comparison with Kilbourne Hole samples of the same lithology.

2.3. Ngaoundéré plateau and Lake Barombi Mbo, Cameroon

The two Cameroonian localities, Ngaoundéré plateau (7°19′40″ N and 13°35′5″ E) and Lake Barombi Mbo (4°39′45″N and 9°24′15″E) are part of the Cameroon Line, a roughly linear 1600 km long Y-shaped volcanic system. The Cameroon Line is a highly unusual intra-plate alkaline volcanic province that transects the ocean-continent boundary (Fitton, 1987) extending from the Ngaoundéré plateau in Nigeria in the northeast, through many volcanic sites in Cameroon, to the Atlantic volcanic islands of Bioko, São Tomé and Príncipe, and Annobón (also known as Pagalu), in the southwest. The origins of the Cameroon Line have been disputed (e.g. Fitton and Dunlop, 1985; Lee et al., 1994; Atouba et al., 2016). The only currently active volcano is Mount Cameroon, which last erupted in 2000 (Suh et al., 2008).

Ultramafic xenoliths from the Cameroon Line comprise largely spinel lherzolites with minor harzburgites and pyroxenites. They are thought to have originated as depleted residues after the extraction of basaltic melts (Lee et al., 1996). Enrichment by small degree partial melts is evidenced in some xenoliths, potentially associated with the breakup of Pangaea (Lee et al., 1996). Major element chemistry suggests some melt depletion has occurred to xenoliths from this locality, however, incompatible elements and isotopic compositions suggest multi-stage depletions and metasomatic enrichments (Lee, 1994).

2.3.1. Ngaoundéré plateau

The Ngaoundéré plateau is built up from Ne-normative alkali basalt flows with a central volcano, Nganha, that produced basanite with minor trachyte and phonolite lavas (Halliday et al., 1988; Lee, 1994). The Nganha flows are dated at between 11 and 7 Ma (Lee, 1994; Marzoli et al., 1999). Geophysical data has suggested that the crust and lithosphere under Ngaoundéré is thinned (Marzoli et al., 1999). Xenoliths from this locality comprise both peridotites and pyroxenites.

Very low equilibration pressures have been estimated for Ngaoundéré spinel lherzolites using the analysis of CaO in olivine by the method of Brey and Köhler (1990), published in Lee (1994). The pyroxenites in this work are thought to be from higher pressures (>1.3 GPa), as assessed by the method of Brey and Köhler (1990) of Al exchange between orthopyroxene and garnet (Lee, 1994). Equilibration temperatures for the spinel lherzolites range from 800 to 1000°C, whereas pyroxenites are from higher temperatures (>960°C) using the method of Brey et al. (1990), published in Lee (1994).

The pyroxenite-forming event at Ngaoundéré has not been extensively studied, and pyroxenite formation from elsewhere in the Cameroon Line has disputed origins. The pyroxenites found in this region have been thought to represent melts crystallized at mantle depth (Kamgang et al., 2013; France et al., 2015); or to be dominated by cumulate-formation processes with some locations inferred to reflect reactive-melt processes (Tedonkenfack et al., 2019). Pyroxenites have also often been invoked as potential source influences in magma generation in this region (Atouba et al., 2016).

Ngaoundéré samples in this work comprised one spinel lherzolite and two pyroxenites. The samples were chosen to avoid any xenoliths with metasomatic phases, and minimalize examples with decomposition of primary phases. Each of the sampled xenoliths from this locality have depletion in both light REE and heavy REE (Lee, 1994).

The spinel lherzolite, P13, is described as fresh, without reaction rims around the grains (Lee et al., 1996). P13 has a porphyroclastic texture, transitional between protogranular and equigranular (Lee, 1994). This sample has 65% olivine, 25% orthopyroxene, 10% clinopyroxene and 5% spinel (Lee, 1994). Both pyroxenite samples are spinel-garnet websterites with/without pargasite (P6/P12). They are described by Lee et al. (1996) as having variable degrees of alteration, and both have 65% clinopyroxene. Pyroxenite, P6, is the only sample from this area of the Cameroon Line that Lee et al. (1996) found to contain amphibole (20%), which may represent modal metasomatism in this sample (Lee, 1994). P6 also contained 5% each of orthopyroxene, garnet, and spinel (Lee, 1994). Pyroxenite P12 has 15% orthopyroxene, and 10% each of garnet and spinel (Lee, 1994). P12 also has examples of secondary carbonate cross-cutting some clinopyroxene grains.

The sample used here was chosen to be comparable with the Kilbourne Hole xenolith suite by including a further examples of spinel lherzolite and pyroxenite.

2.3.2. Lake Barombi Mbo

Lake Barombi Mbo is a Quaternary maar, ~54 km NE of Mount Cameroon. The deposits are dominantly basaltic pyroclastics (Chako Tchamabe et al., 2013). Xenoliths from this locality comprise both peridotites and pyroxenites (Chako Tchamabe et al., 2013). Some Barombi Mbo xenoliths record a small degree of partial melting (Pintér et al., 2015). The majority of Barombi Mbo xenoliths are slightly enriched in fertile major elements relative to similar xenoliths from nearby Nyos (Pintér et al., 2015). The estimated equilibration pressures for spinel lherzolite from this locality are extremely low (Lee, 1994), as calculated from by analysis of CaO in olivine by the method of Brey and Köhler (1990). This may suggest reequilibration at a shallow crustal depth, or greater unreliability of the geobarometers available for spinel peridotites. Equilibration temperatures for spinel lherzolites are comparable to those calculated for Ngaoundéré (Lee, 1994), using 2 pyroxenes method of (Brey et al., 1990).

Xenoliths from this locality are hosted in an explosive breccia layer (Chako Tchamabe et al., 2013). They have protogranular and porphyroclastic textures, and as elsewhere in the Cameroon Line, show evidence for having small degrees of melt extraction (Pintér et al., 2015). No chemical zoning is observed in olivines (Lee, 1994).

The spinel lherzolite C235D had no metasomatic phase and is described as unmetasomatised (Lee, 1994), and has a protogranular texture (Lee, 1994). Modal mineral compositions have been estimated as 60% olivine, 25% orthopyroxene, 10% clinopyroxene and <5% spinel (Lee, 1994).

The sample used here was chosen to be comparable with the Kilbourne Hole xenolith suite by including a further example of spinel lherzolite.

3. ANALYTICAL METHODS

The ultramafic samples used for bulk rock analysis in this study were previously prepared powders, with the exception of Labait Hill xenoliths and the Cameroonian pyroxenites, which were fine crushates. The Kilbourne Hole samples were prepared recently in a metal-free environment and powdered using an agate ball mill to avoid metal contamination. Preparation techniques for other xenoliths are not known. The samples used for individual mineral analysis were hand-picked under 50× magnification from crushate, to exclude alteration, inclusions, composite grains, surficial adherents, or weathered edges.

Analytical work was completed in the Department of Earth Sciences, University of Oxford. All mineral acids used in sample dissolution, column chemistry, and analysis were distilled in house by sub-boiling and diluted by volume with ultrapure 18 MΩ•cm water. For bulk rocks ~0.010 g was accurately weighing into Savillex® PFA vials. For mineral separates only enough material was weighed to give ~1000 ng natural Ni. Samples were digested in 2 stages; first using a total of 2 ml HNO_3:HF mixed acid (3:1), on a hotplate. After this first stage was evaporated, sufficient 6 M HCl, (up to 5 ml) to bring the sample back into solution was added. For all bulk rocks and spinel separates, the 6 M HCl stage was conducted with the Savillex vial placed into a Parr High Pressure Acid Digestion vessel at 180 °C, until an optically clear solution was obtained (>3 days). Silicate mineral separates were dissolved entirely by hotplate dissolution. After dissolution, a double spike consisting of 25:75 ^{61}Ni:^{62}Ni was added to an aliquot of each sample, both accurately weighed. A ratio of 2.5 parts double spike Ni to 1 part natural Ni was used (Gall et al., 2012) to give a total of 3850 ng Ni in each sample.

Nickel purification was carried out in a metal-free laboratory using the three stage ion exchange chemistry of Gall et al. (2012). The method was modified to increase the volume of the first load solution in order to increase the capacity of Ca and Mg to be removed by the first column. Additional HNO_3 was added and dried down before final dry down and dilution for analysis in order to destroy column-related organics.

Nickel isotopes (58, 60, 61, and 62) were analysed in pseudo-high resolution on a Nu Plasma HR MC-ICPMS, with each collector using a $10^{11}\Omega$ resistor, capable of measuring currents up to 10^{-10}A. Each run included an ESA deflected baseline followed by a peak centre, offset, and then 30 ratios, with 15 second integration time. The analysed masses were measured on the peak shoulders in order to avoid variable polyatomic interferences, especially on mass 58. Mass 57 was monitored for correction of the isobaric interference of ^{58}Fe on ^{58}Ni. Two natural FeNi-sulphides were used as in-house standards to monitor the correction of the polyatomic and isobaric interferences. These were measured both unpurified (with Fe) and purified through column chemistry (no Fe). To further reduce the effect of any residual uncorrected polyatomic interferences or matrix effects, samples and standards were intensity matched at a total Ni signal of ~15 V. Data reduction for the deconvolution of the double spike was done online following the procedures of Siebert et al. (2001). Isotope compositions are reported as $\delta^{60/58}$Ni per mil (‰) deviations relative to SRM986. Nickel concentrations were calculated by isotope dilution from the fractionation corrected double spiked data.

The accuracy and precision of our methods were assessed by repeated analysis of USGS reference materials in each analytical session. At least one USGS reference material (BHVO2, BIR1a, PCC1, or DTS2) was processed with each sample batch and analysed over more than one session. Average $\delta^{60/58}$Ni and 2× standard deviation (2SD) for these rock standards are reported in Table 1. All are within error of the published values, except for the PCC1 value of Cameron et al. (2009), which is outside the range of all subsequent studies, with which our value agrees.

Based on the repeated analyses of rock standards (Table 1) we assess external reproducibility during this study, as ±0.06‰ (2SD). This uncertainty is used for all representative error bars in the figures in this work. Klaver et al. (2020) reported 2× standard error of the mean (2SE), of separate analyses. This approach is unusual in the literature as standard deviation (SD) is a measure of the amount of variability, or dispersion of data from the mean, while the standard error (SE) of the mean measures how far the given mean of the data is likely to be from the true population mean. In order to compare the data of Klaver et al. (2020) with our data in Fig. 2, the reported 2SE have been recalculated to 2SD (i.e. multiplied by $\sqrt{n}$ where n is the value reported in Table 1 of Klaver et al. (2020)). We note that the resulting 2SD are an improvement by a factor of 2 on our 2SD external reproducibility, probably reflecting 3-fold higher Ni signal (50–85 V vs 15 V) measured by Klaver et al. (2020).

A total procedural Ni blank was processed with each batch of column chemistry to monitor all potential Ni contamination. These blanks were analysed by ICP-MS on a Thermo-Finnigan™ Element 2, or a PerkinElmer™ NexION Quad 350D and were always <3.6 ng. This is insignificant given that the total natural sample Ni was always >995 ng.

4. RESULTS

Bulk rock nickel isotopic compositions and concentrations for 24 peridotites and 5 pyroxenites are presented in Table 2, and graphically Fig. 2. Results for mineral separates are presented in Table 3, and graphically in Fig. 3 and Fig. A3. The minerals comprise olivine (n = 4), orthopyroxene (n = 6), clinopyroxene (n = 6), and spinel (n = 2), from five rocks from Kilbourne Hole and Cameroon.

4.1. Bulk rocks

The Ni concentrations of the peridotite xenoliths analysed in this study range from 1394 to 2597 μg g^{-1}, the average of which (1986 μg g^{-1}, n = 24) is only slightly higher than the 1960 μg g^{-1} estimated for the Primitive Mantle, (McDonough and Sun, 1995). Bulk rock analyses of $\delta^{60/58}$Ni in peridotite xenoliths range from +0.02‰ to +0.26‰. Pyroxenite xenoliths have a slightly wider range in Ni concentrations, from 233 to 1757 μg g^{-1} (n = 5), with bulk rock $\delta^{60/58}$Ni ranging from −0.38‰ to +0.16‰. There is no correlation between Ni isotopic composition and Ni concentration (Fig. A4).

There is no resolvable difference between the Ni isotopic compositions of comparable lithologies at the three locations sampled in this work (Fig. 2). The $\delta^{60/58}$Ni compositions of garnet lherzolites (+0.17‰ and +0.24‰, n = 2), spinel harzburgites (range +0.09‰ to +0.23, n = 4), and dunites (+0.10‰ to +0.13‰, n = 2) are within the range of the spinel lherzolites (+0.02‰ to +0.26‰, n = 16). Pyroxenites have the widest range in $\delta^{60/58}$Ni compositions (−0.38‰ to +0.16‰, n = 5). Recent work by Klaver et al. (2020) also observed no resolvable difference in $\delta^{60/58}$Ni between lithologies from five additional localities (Fig. 2). Comparable $\delta^{60/58}$Ni compositions were observed between garnet lherzo-

Table 1
Published values for $\delta^{60/58}$Ni of selected USGS reference materials, in ‰ normalised to NIST SRM986, compared to this work.

	BIR1a			BHVO2			PCC1			DTS2		
	$\delta^{60/58}$Ni	2SD	n	$\delta^{60/58}$Ni	2SD	n	$\delta^{60/58}$Ni	2SD	n	$\delta^{60/58}$Ni	2SD	n
Cameron et al. (2009)				**+0.13**	0.03	NR	**+0.34**	0.08	NR			
Gall et al. (2012)	**+0.13**	0.07	68	**+0.05**	0.07	90	**+0.12**	0.07	34			
Steele et al. (2012)										**+0.128**	0.08*	NR
Gueguen et al. (2013)	**+0.12**	0.04	3	**+0.01**	0.04	11	**+0.12**	0.05	5			
Ratié et al. (2015)				**+0.01**	0.02	4						
Chernonozhkin et al. (2015)	**+0.191**	0.066	2	**+0.083**	0.019	5	**+0.166**	0.048	8			
Gall et al. (2017)							**+0.141**	0.056	17			
Pašava et al. (2019)				**+0.015**	0.05	5						
Klaver et al. (2020)							**+0.132**	0.025[a]	8	**+0.131**	0.025[a]	8
This study	**+0.142**	0.057	20	**+0.026**	0.059	36	**+0.140**	0.060	17	**+0.152**	0.049	13

Values in bold are to emphasize the actual delta value, over the errors etc.
2SD = 2 × standard deviation.
NR = Not reported.
2SD is uncertainty as 2 times the standard deviation of the individual measurements of each sample. In this work ±0.06‰ is used as representative of the external reproducibility.
For this work 'n' represents the total number of analyses from multiple runs of each sample. PCC1 and DTS2 is the same dissolution with separate chemistry, BHVO2 and BIR1a are from numerous dissolutions.
* 2SE reported only, without n.
[a] calculated from reported $2s_{\bar{x}} = 0.009$, by multiplication with $\sqrt{n}$, where n = 8.

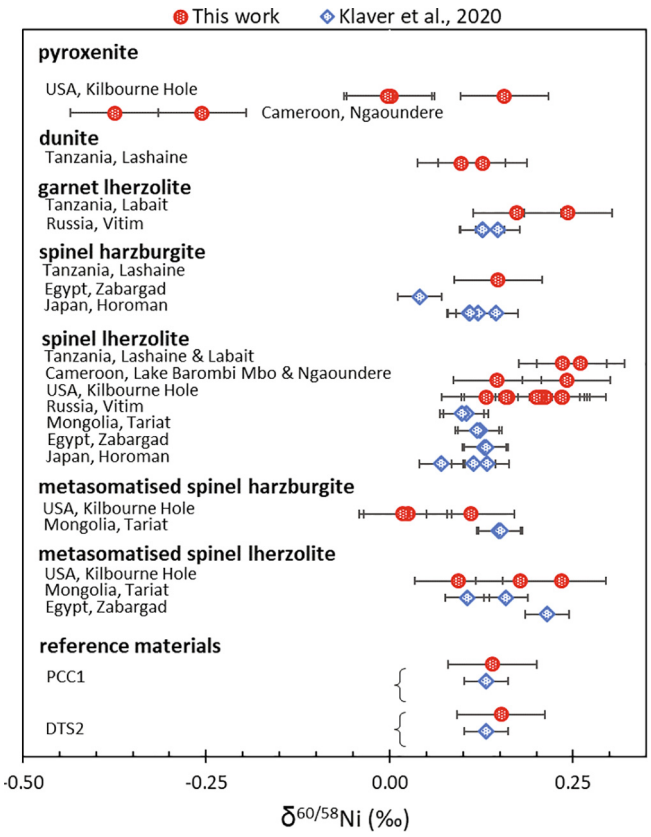

Fig. 2. Bulk rock $\delta^{60/58}$Ni for peridotites from this work compared to the recent Klaver et al. (2020) data. The $\delta^{60/58}$Ni compositions for lithological groups do not vary significantly with location. Samples identified as metasomatised are those showing petrographic evidence of minor metasomatism (Harvey et al., 2012; Klaver et al., 2020). The error bar shows the 2SD external reproducibility from repeated analyses of USGS reference materials (±0.06‰) for this study and comparable 2SD error on repeated analyses of USGS reference materials (±0.03‰) for Klaver et al. (2020).

lites (range +0.13‰ to +0.15‰, n = 3); spinel harzburgites (range +0.11‰ to +0.15‰, n = 5); and spinel lherzolites (range +0.04‰ to +0.22‰, n = 9) (Klaver et al., 2020).

Kilbourne Hole is the most sampled locality in this work (n = 18). The majority of samples from Kilbourne Hole are spinel lherzolites, with an average $\delta^{60/58}$Ni of +0.16 ± 0.14‰ (2SD, n = 12). The harzburgites from Kilbourne Hole, although fewer in number, have a comparable average and variance of $\delta^{60/58}$Ni of +0.17 ± 0.12‰ (2SD, n = 3). Three pyroxenites were also analysed from Kilbourne Hole: average $\delta^{60/58}$Ni = +0.05 ± 0.15‰ (2SD, n = 3). Two of the pyroxenites have $\delta^{60/58}$Ni = +0.00‰, much lighter than the average peridotite samples from this locality. The third sample is the only one that contains spinel and has a heavier $\delta^{60/58}$Ni of +0.16‰.

Six peridotites from Kilbourne Hole have minor metasomatic features (Harvey et al., 2012). If these are excluded the range of $\delta^{60/58}$Ni for unmetasmonatised peridotites reduces to +0.13‰ to +0.24‰. The samples with metasomatic features extend to significantly lighter values (+0.02‰ to +0.23‰). The sample set of Klaver et al. (2020) also includes peridotites with petrographic indicators of metasomatism. The $\delta^{60/58}$Ni of these samples extend to heavier values (+0.11‰ to +0.22‰) than those of their unmetasomatised counterparts (+0.04‰ to +0.15‰).

In addition to the petrographic indicators of metasomatism, the intensity of post melt-depletion metasomatic processes affecting Kilbourne Hole has been characterised using $(La/Yb)_N$, (Harvey et al., 2015). Peridotites with $(La/Yb)_N > 1$ are thought to have experienced higher degrees of silicate metasomatism, than those with $(La/Yb)_N < 1$. Peridotites with $(La/Yb)_N > 1$ span the whole range in peridotite $\delta^{60/58}$Ni at this locality (+0.02‰ to +0.24‰).

Cameroonian xenoliths shows the widest range in $\delta^{60/58}$Ni (see Fig. 2), despite having the least samples analysed. Spinel lherzolites from the Cameroon Line have $\delta^{60/58}$Ni within the range of $\delta^{60/58}$Ni values for spinel lherzolites from Kilbourne Hole (+0.24‰, Lake Barombi Mbo; +0.15‰, Ngaoundéré). The two pyroxenites from Ngaoundéré have extremely light $\delta^{60/58}$Ni (P6: −0.26‰; P12: −0.38‰), even compared with the Kilbourne Hole pyroxenites (average +0.05 ± 0.15‰, 2SD, n = 3).

Tanzania has the smallest range in $\delta^{60/58}$Ni of the localities analysed in this work (+0.10‰ to +0.26‰, n = 7). The Tanzanian spinel lherzolites from Labait Hill ($\delta^{60/58}$Ni = +0.24‰) and Lashaine ($\delta^{60/58}$Ni = +0.26‰) are indistiguishable within error, and heavier than the majority of Kilbourne Hole spinel lherzolites. The harzburgite from Lashaine, Tanzania ($\delta^{60/58}$Ni = +0.15‰) is within the

Table 2
Nickel isotopic compositions and Ni concentrations in ultramafic xenoliths.

Sample	Lithology	Indicator of metasomatism[a]	[Ni] (μg g^{-1})	$\delta^{60/58}$Ni (‰)	2SD	n
Kilbourne Hole, New Mexico						
KH03-11	Spinel lherzolite		1984	+0.161	0.052	3
KH03-06	Spinel lherzolite		1769	+0.209	0.030	3
KH03-07	Spinel lherzolite		1829	+0.212	0.047	3
KH96-18	Spinel lherzolite		1578	+0.235	0.029	4
KH03-02	Spinel lherzolite		2070	+0.131	0.069	5
KH03-25	Spinel lherzolite		2195	+0.205	0.039	5
KH96-2	Spinel lherzolite		2497	+0.158	0.078	3
KH03-10	Spinel lherzolite	×	2003	+0.111	0.064	5
KH03-21	Spinel lherzolite	×	1612	+0.025	0.034	5
KH03-03	Spinel lherzolite		1628	+0.235	0.038	3
KH96-8	Spinel lherzolite		1862	+0.199	0.033	3
KH03-24	Spinel lherzolite	×	1680	+0.018	0.034	4
KH03-27	Spinel harzburgite	×	2198	+0.094	0.047	5
KH03-15	Spinel harzburgite	×	1923	+0.178	0.064	4
KH03-16	Spinel harzburgite	×	2203	+0.234	0.050	3
KHPX13-06	Pyroxenite with minor spinel		632.6	+0.156	0.022	3
KHPX13-10	Pyroxenite with minor olivine		232.9	+0.002	0.036	3
KHPX13-22	Pyroxenite with minor olivine		1757	−0.003	0.046	2
Lashaine, Tanzania						
BD774	Spinel lherzolite		2244	+0.260	0.012	3
BD822	Spinel harzburgite		2359	+0.148	0.044	5
BD806	Fe-rich Ti-biotite-bearing dunite		1394	+0.127	0.058	3
BD825	Spinel dunite		1552	+0.098	0.053	3
Labait, Tanzania						
H93-X1	Garnet lherzolite		2597	+0.243	0.031	4
H93-X9	Garnet lherzolite		2575	+0.173	0.073	3
H93-X8	Spinel lherzolite		2303	+0.236	0.036	4
Ngaoundéré, Cameroon						
P6	Spinel-garnet-pargasite websterite	×	462.7	−0.256	0.007	2
P12	Spinel-garnet websterite		442.7	−0.375	0.028	6
P13	Spinel lherzolite		1978	+0.147	0.047	6
Lake Barombi Mbo (nr Mt Cameroon)						
C235D	Spinel lherzolite		1645	+0.241	0.042	5

Values in bold are to emphasize the actual delta value, over the errors etc.
Ni concentration measured by isotope dilution.
Reported 2SD is calculated from repeated analyses of specific samples, in many cases this value is less than the external reproducibility of Ni isotopic composition ±0.06‰.
n is the number of separate analyses of the sample. Samples analysed more than three times were also analysed from duplicate dissolutions.
[a] Indicators of metasomatism are petrographic: interstitial glass and reaction rims around grains of clinopyroxene (Harvey et al., 2012); and presence of amphibole (P6; Lee, 1994).

range of Kilbourne Hole harzburgites. The only examples of garnet lherzolites in this work are both from Labait Hill, Tanzania. These samples have $\delta^{60/58}$Ni of +0.24‰ and +0.17‰, the heavier value of which is identical to the spinel lherzolite from the same locality. The two dunites from Lashaine, Tanzania analysed in this work have lighter $\delta^{60/58}$Ni compositions (+0.13‰ and +0.10‰) than other lithologies from the same locality. These values plot between the $\delta^{60/58}$Ni of altered (+0.06‰) and unaltered (+0.20‰) dunites of Spivak-Birndorf et al. (2018).

4.2. Mineral separates

Regardless of the bulk rock Ni isotopic composition, there is a small, near constant difference of between +0.09‰ and +0.12‰ between the $\delta^{60/58}$Ni of the heaviest and lightest mineral phases in each of the analysed xenoliths. Where analysed, spinel is the heaviest phase.

The major minerals of peridotite xenoliths that do not exhibit petrographic indicators of metasomatism (Kilbourne Hole n = 2; Cameroon n = 1) have $\delta^{60/58}$Ni indistinguishable at even the 2σ level (Fig. 3). Clinopyroxenes in these xenoliths have an average $\delta^{60/58}$Ni of +0.06 ± 0.03‰ (2SD), which is consistently lighter than the average of $\delta^{60/58}$Ni of olivines and orthopyroxenes, which are identical, (average +0.17 ± 0.02‰, 2SD).

Major mineral phases from the peridotite xenoliths that do exhibit petrographic indicators of minor metasomatism (Kilbourne Hole, n = 2) also show the same differences between mineral phases with clinopyroxene being lighter than olivine and orthopyroxene, which are identical within error for any specific xenolith. The only examples of spinel

Table 3
Nickel isotopic compositions and Ni concentrations from mineral separates.

Mineral	[Ni] (μg g^{-1})	$\delta^{60/58}$Ni (‰)	2SD	n
Kilbourne Hole, New Mexico, USA				
KH03-25, Group 1 spinel lherzolite				
Olivine	2745	+0.172	0.045	5
Orthopyroxene	731.1	+0.152	0.025	5
Clinopyroxene	327.8	+0.048	0.007	2
KH03-06, Group 2 spinel lherzolite				
Olivine	2597	+0.161		1
Orthopyroxene	711.9	+0.183		1
Clinopyroxene	336.7	+0.076	0.024	2
KH03-24, Group 2 harzburgite				
Olivine	2384	−0.021	0.018	3
Orthopyroxene	661.3	−0.041		1
Clinopyroxene	323.5	−0.082	0.020	3
Spinel	2057	+0.032	0.022	4
KH03-27, Group 1 harzburgite				
Olivine	2714	+0.094	0.046	3
Orthopyroxene	1590	+0.083	0.012	3
Clinopyroxene	243.4	+0.036	0.012	3
Spinel	2133	+0.128	0.079	6
Cameroon Line				
C235D, spinel lherzolite, Lake Barombi Mbo				
Orthopyroxene	631.9	+0.173	0.010	2
Clinopyroxene	262.4	+0.070	0.021	2
P6, spinel garnet pargasite websterite, Ngaoundéré				
Orthopyroxene	625.1	−0.311	0.037	4
Clinopyroxene	270.1	−0.235	0.006	4

Values in bold are to emphasize the actual delta value, over the errors etc.
Ni concentration calculated by isotope dilution. External reproducibility of Ni isotopic composition ±0.06‰. n is the number of separate analyses of the sample. Samples analysed more than three times were also analysed from duplicate dissolutions.

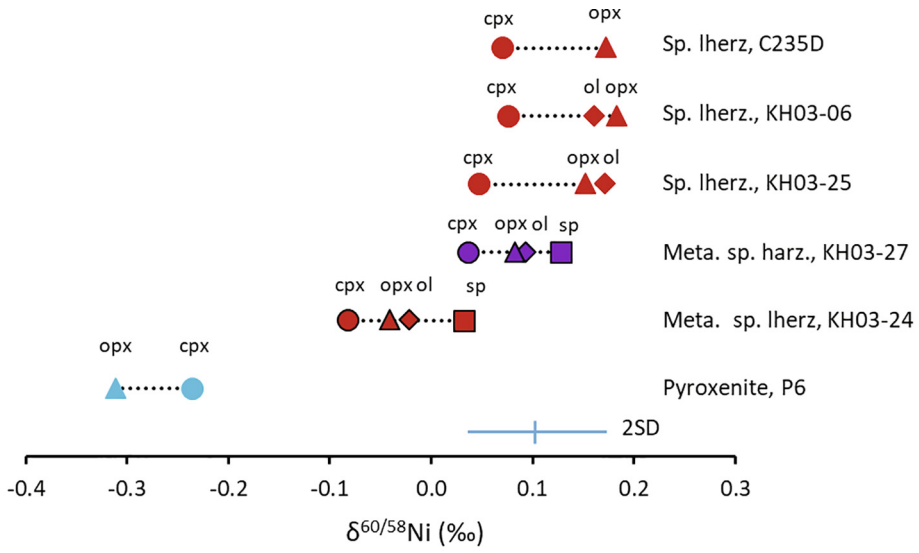

Fig. 3. $\delta^{60/58}$Ni for mineral separates from peridotite xenoliths analysed in this work. Despite the small and constant range, the differences between minerals are systematic. Abbreviations: meta. = petrographic indicators of metasomatism (highlighted by black outline), sp. lherz = spinel lherzolite (red); sp. harz. = spinel harzburgite (purple); pyroxenite = websterite (blue). C235D & P6 = Cameroon Line; KH03-XX = Kilbourne Hole. External reproducibility (±0.06‰) represented with the error bar presented. (For interpretation of the references to colour in this figure legend, the reader is referred to the web version of this article.)

analysed in this work was from these samples, and in each case was the heaviest phase in the xenolith. In each of these xenoliths, the mineral phases possess lighter $\delta^{60/58}$Ni than the same phases in apparently unmetasomatised xenoliths, and there is no consistent $\delta^{60/58}$Ni composition for any single mineral phase between xenoliths. Therefore, the xenoliths appear to be in Ni isotopic equilibrium internally, despite the presence of metasomatic features.

Ni isotopic compositions were also analysed for pyroxenes separated from one of the Ngaounderé, Cameroon pyroxenites (P6). In this sample, $\delta^{60/58}$Ni of orthopyroxene (−0.31‰) was lighter than the co-existing clinopyroxene (−0.27‰). The mineral separates (orthopyroxene and clinopyroxene) from pyroxenite P6 agree with the bulk composition, suggesting little influence on the bulk from any alteration excluded from the minerals. However, orthopyroxene and clinopyroxene only account for 70–75% of the estimated modal mineralogy of this sample: 65–70% clinopyroxene, ≤5% orthopyroxene, ≤20% amphibole, ≤5% of spinel, and ≤5% garnet (Lee et al., 1996). Nickel contents of amphibole (12–200 μg g^{-1}; Wedepohl, 1974) and garnet (40–200 μg g^{-1}; Wedepohl, 1974) are unlikely to contribute significantly to the Ni budget of this sample.

Klaver et al. (2020) report $\delta^{60/58}$Ni for five olivine and bulk rock pairs. These showed limited differences between the $\delta^{60/58}$Ni of the host bulk rock and of the olivine separate (≤0.03‰). No other mineral separates were analysed. In contrast to this work, olivine is heavier in $\delta^{60/58}$Ni than the host bulk rock, for four of the five olivine and whole rock pairs. However, in both this work and for all but one example in Klaver et al. (2020), the differences between olivine and bulk rock are within their respective external reproducibility.

5. DISCUSSION

The range in $\delta^{60/58}$Ni compositions is very similar in peridotite xenoliths from Cameroon Line and from Tanzania (~0.10‰); a greater range is seen in Kilbourne Hole ~0.24‰). The range in $\delta^{60/58}$Ni compositions observed in other localities reported in the literature is comparable (up to 0.17‰; Klaver et al., 2020). The process producing heterogeneity in $\delta^{60/58}$Ni appears to global.

In the following, we discuss some key features of data that shed light on the causes of the Ni isotope variations outlined above. We start with the mineral data and then explore the causes of the light $\delta^{60/58}$Ni in some bulk peridotites. We finish by discussing the implications for the $\delta^{60/58}$Ni of the bulk silicate earth.

5.1. Equilibrium Ni isotope fractionation between major mantle minerals

Previously published $\delta^{60/58}$Ni for mantle minerals are limited (see Section 1). Variation in mineralogy or mineral fractionation is incapable of producing significant change in bulk rock $\delta^{60/58}$Ni because the inter-mineral fractionation is so small. Modelling of melting in the mantle using the equations of Shaw (1979), with an $\alpha_{(\text{residue-melt})}$ calculated from the published BSE $\delta^{60/58}$Ni = +0.12‰ of Klaver et al. (2020), and the average of published $\delta^{60/58}$Ni MORB data = +0.02‰ (Cameron et al., 2009; Gall, 2011; Gueguen et al., 2013), and bulk D calculated from mantle modal mineralogy and $D_{\text{mineral-liquid}}$ of Ni from Putirka et al. (2011) shows that even 40% melting is unable to produce greater $\delta^{60/58}$Ni fractionation than 0.01‰. This is well within analytical uncertainty and far below the $\delta^{60/58}$Ni fractionation observed in the mantle xenoliths. Such observations are in complete agreement with the melting model of Klaver et al. (2020), which found $\delta^{60/58}$Ni insensitive to melt depletion.

Minerals sampled here appear to reflect isotopic equilibrium in $\delta^{60/58}$Ni. However, direct determination of isotopic equilibrium can only be obtained from time series and reversal experiments, or by the three isotope method (Young et al., 2002). Evidence for isotopic inter-mineral equilibrium is provided by the trends defined by the different silicate mineral phases, such as with Fe (Fig. A5a), and with Ni/(Ni + Fe + Mg) (Fig. A5b). This is comparable to the test used in (Zhao et al., 2017). Evidence of isotopic equilibrium is also provided by the isotopic compositions of mineral pairs, as used to establish isotopic equilibrium for Fe isotopes (Sossi et al., 2012). A strong positive relationship between the $\delta^{60/58}$Ni of each silicate phase pair is observed (Fig. 4), rather than any evidence of the perpendicular trend associated with kinetic isotope fractionation (Sossi et al., 2012, Fig. 6). Kinetic isotope effects caused by element diffusion, which generate large isotopic variations (Zhao et al., 2017), can be an order of magnitude larger than equilibrium fractionations (Klaver et al., 2020). The observed inter-mineral fractionation in this work is small and consistent, unlike fractionation generated by kinetic processes.

Most minor phases (unsampled) host insufficient Ni and/or are too small in modal abundance to account for the variations in xenolith $\delta^{60/58}$Ni. Garnet ([Ni] = 40–200 μg g^{-1}; Wedepohl, 1974) is either absent in most xenoliths, or <10% modal composition. Garnet would need to have an extreme $\delta^{60/58}$Ni to significantly affect the bulk rock $\delta^{60/58}$Ni, which is not expected from the agreement of $\delta^{60/58}$Ni of bulk spinel lherzolites and garnet lherzolites. Sulphide minerals in the mantle are modally extremely minor, however may potentially influence bulk rock mantle $\delta^{60/58}$Ni because there are many sulphide species that have integral Ni in their formulae. Published $\delta^{60/58}$Ni for sulphides (Fig. 1) have shown highly variable $\delta^{60/58}$Ni of −1.05‰ to +0.76‰, (Tanimizu and Hirata, 2006; Gall, 2011; Gueguen et al., 2013; Hofmann et al., 2014). For Kilbourne Hole peridotites, sulphide constitutes only 0.03 wt%, with Ni-bearing sulphides being a small subset of this amount (Harvey et al., 2011). Bulk rock S contents in Kilbourne Hole peridotites do not exceed 130 μg g^{-1} (Harvey et al., 2015), relative to the primitive mantle value of 250±50 μg g^{-1} (Lorand, 1990; O'Neill, 1991; Palme and O'Neill, 2007). Lack of sulphide control on bulk rock Ni isotopes is consistent with the absence of any $\delta^{60/58}$Ni relationship with sulphur concentration (Fig. A6).

The bulk rock Ni isotope composition calculated from combining the mineral separate compositions and modal

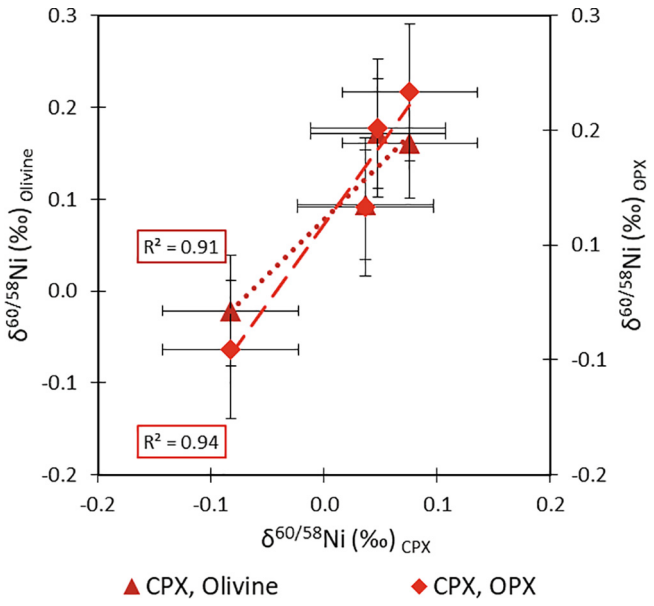

Fig 4. $\delta^{60/58}$Ni of mineral phases from xenoliths from Kilbourne Hole. Strong positive trends are associated with isotopic equilibrium, (e.g. Sossi et al., 2012). External reproducibility of the Ni isotopic compositions is ±0.06‰.

mineralogy is the same as the measured composition from measuring a bulk rock powder, for xenoliths where all mineral phases were measured (Table 4). These successful reconstructions by mass balance also provide evidence that the bulk rock compositions are not perturbed by surficial alteration, interstitial glass, or minor minerals (e.g. sulphide), which might be sampled in bulk rock analyses but not in the pure mineral separates.

For each mineral analysed in this work, Ni would be hosted in an octahedral site, so the limited range observed between the $\delta^{60/58}$Ni of these phases is not unexpected. No correlations were found between bulk rock $\delta^{60/58}$Ni and modal mineralogy in this work (Fig. A7, providing evidence that mantle $\delta^{60/58}$Ni do not reflect varying proportions of minerals with inherently distinct $\delta^{60/58}$Ni.

With the exception of the Cameroon pyroxenite, clinopyroxene is consistently the lightest phase in $\delta^{60/58}$Ni, spinel is the heaviest (where analysed). The $\delta^{60/58}$Ni in orthopyroxene and olivine are consistently almost identical, where both phases are analysed from the same xenolith. The lattice sites available for Ni substitution are extremely similar in these two Fe-Mg silicates, producing approximately identical isotopic fractionation. The clinopyroxenes in the Kilbourne Hole peridotites are predominantly Cr-diopside, which is a Cr-bearing Ca-(Mg,Fe) silicate (Deer et al., 1966), and in the pyroxenites the clinopyroxenes are predominantly Al-rich augite, a Al-bearing (Ca, Na)-(Mg,Fe) silicate. The addition of Ca, which is a larger ion (Shannon, 1976), into the structure may be responsible for the different fractionation in Ni that produces consistently lighter $\delta^{60/58}$Ni. Spinels are not silicates, and the absence of the SiO_4 tetrahedra, which changes the bond stiffness, may be responsible for the consistently heavy $\delta^{60/58}$Ni in this mineral.

Table 4
Reconstruction of the Ni isotopic composition of the bulk xenoliths from modal mineralogy and Ni isotopic composition of analysed mineral separates, compared to the analysed bulk rock.

		Actual		Reconstruction	
	Modal %	[Ni] (μg g^{-1})	$\delta^{60/58}$Ni (‰)	[Ni] (μg g^{-1})	$\delta^{60/58}$Ni (‰)
KH03-24		**1680**	**+0.02**	**1625**	**−0.02**
Olivine	56.4	2384	−0.02		
Orthopyroxene	13.2	324	−0.08		
Clinopyroxene	27.8	661	−0.04		
Spinel	2.6	2057	+0.03		
KH03-27		**2198**	**+0.09**	**2453**	**+0.09**
Olivine	79.1	2714	+0.09		
Orthopyroxene	2.2	243	+0.04		
Clinopyroxene	18.9	1590	+0.08		
Spinel	0	2133	+0.13		

Values in bold are to emphasize the actual delta value, over the errors etc.
Ni concentration calculated by isotope dilution. External reproducibility on analysed Ni isotopic composition is ± 0.06‰.
Modal mineralogy from Harvey et al. (2012).

Interestingly, the $\delta^{60/58}$Ni fractionation between clinopyroxene and orthopyroxene ($\Delta^{60/58}Ni_{cpx\text{-}opx}$) varies systematically with their chemistry. Specifically, the magnitude of $\Delta^{60/58}Ni_{cpx\text{-}opx}$, co-varies negatively with the Fe/Mg and positively with Si/Fe, of both clinopyroxene and orthopyroxene (Fig. 5). Additionally, $\Delta^{60/58}Ni_{cpx\text{-}opx}$ also co-varies (Fig. 5) with CaO/Al_2O_3, La/Yb, Sm/Nd in clinopyroxene and with MnO, TiO_2 in orthopyroxene. Further, the $\Delta^{60/58}Ni_{cpx\text{-}opx}$ also co-varies with some bulk rock geochemical indicators including $\delta^{60/58}$Ni (Fig. 7), as well as U concentration, La/Yb, and Sm/Nd (Fig. 6). Clinopyroxene usually hosts the majority of the incompatible elements in spinel lherzolites (Lee, 1994), which could be responsible for the stronger relationships in this phase, and the relationships with bulk rock compositions limited to those elements enriched in clinopyroxene. It appears that this equilibrium isotopic fractionation is a function of mineral chemistry. This fractionation is additionally related to parameters normally associated with trace element enrichment and fertility. No trend is observed with the $\delta^{60/58}$Ni fractionation between clinopyroxene and olivine (Fig. A9).

Since $\delta^{60/58}$Ni mantle heterogeneity is not caused by fractionation between constituent mineral phases, the variability must reflect some other process.

5.2. Isotopically light $\delta^{60/58}$Ni in the terrestrial mantle – a signature of recycling?

Evidence for the lack of control of partial melting on bulk rock $\delta^{60/58}$Ni, further to the too small inter-mineral fractionation, is found in the lack of covariation of $\delta^{60/58}$Ni with indices of partial melting. For example, Cr# in spinel has been suggested to be a proxy for partial melting in ultramafic rocks (Hellebrand et al., 2001) and shows no trend with bulk Ni isotopic composition (Fig. A8). Similarly, there is no evidence to suggest fractional crystallisation affects $\delta^{60/58}$Ni, as there is no trend with Ni concentration (Fig. A4) or MgO content.

One possible cause of the heterogeneity observed in ultramafic xenoliths may be metasomatism. However, samples with petrographic indicators of metasomatism, from this work and Klaver et al. (2020), range from $\delta^{60/58}$Ni = +0.02‰ to +0.23‰, which predominantly overlaps with $\delta^{60/58}$Ni data for unmetasomatised xenoliths: +0.04‰ to +0.26‰. If metasomatism was the direct cause of the heterogeneity a difference between these sample sets would be expected. The lack of a difference provides evidence that this mechanism does not systematically alter bulk ultramafic rock $\delta^{60/58}$Ni composition.

Metasomatism in the Kilbourne Hole peridotites was previously studied by Harvey et al. (2015), who used $(La/Yb)_N$ to broadly segregate Kilbourne Hole peridotites. An elevated LREE/HREE signature, $(La/Yb)_N > 1$, is attributed to recent cryptic metasomatism. In this study, the whole range of $\delta^{60/58}$Ni from this suite of ultramafic rocks is spanned by samples with $(La/Yb)_N > 1$ (open symbols on Figs. 8, 10, and A6) which are the samples that should have more influence from recent metasomatism. Based on the existing data therefore, it seems that metasomatism is unlikely to cause systematic variations in bulk rock $\delta^{60/58}$Ni composition of peridotites.

Subduction of recycled crust may introduce components to the upper mantle via either metasomatism or bulk addition, thereby generating isotopic and chemical heterogeneity. It has been proposed that subduction may induce Mo isotope fractionation (isotopically light Mo enriched in secondary minerals within the subducting slab; König et al., 2016), and potentially also Fe (isotopically light Fe enriched in sulfide melts; Williams et al., 2018). In these examples, the fractionation occurs during dehydration and/or melting of the slab. At present, it is not known if analogous $\delta^{60/58}$Ni fractionation takes place in the subduction zone environment, or if direct input of subducted material with a fractionated light $\delta^{60/58}$Ni, could be responsible for the observed spread in $\delta^{60/58}$Ni in mantle xenoliths. However, there is circumstantial evidence that recycled components could play a role.

From approximately 140 Ma years ago, the oceanic Farallon plate subducted beneath the North American continental margin affecting mantle beneath Kilbourne Hole (Kil and Wendlandt, 2007). During this period, it has been suggested an enrichment process occurred, involving the reaction of a K-rich metasomatic agent (suggested to be potentially related to an old subducted slab) with a depleted MORB-type mantle (Kil and Wendlandt, 2007). Slab-derived metasomatic agents have also been proposed to have affected the mantle beneath Lashaine by production of silicic fluids (Gibson et al., 2013).

Despite the lack of relationships with other major elements, the Fe concentration in Kilbourne Hole bulk peridotite co-varies inversely with bulk rock $\delta^{60/58}$Ni (Fig. 8a). With the exception of one depleted pyroxenite, the trend is continued with the inclusion of pyroxenites from this locality (Fig. 8b). This relationship is also observed in 3 of the 4 localities studied in Klaver et al. (2020), (Horoman, Tariat, and Vitim, plotted in Fig. A10), including a site with examples of petrographic evidence of metasomatism. The combined dataset (n = 40) of peridotites and Fe-rich Kilbourne Hole pyroxenites from this work and peridotites from Klaver et al. (2020) shows a significant relationship (Fig. 4c). However, $\delta^{60/58}$Ni of Cameroon Line websterites and Tanzanian dunites (Fig. 4d) are not consistent with this relationship. Note that the trend between mineral $\delta^{60/58}$Ni and [FeO] (Fig. A11) is the opposite to that in the bulk rocks, providing further evidence the bulk rock $\delta^{60/58}$Ni is not controlled by modal mineralogy.

The relationship between bulk rock $\delta^{60/58}$Ni and [Fe] for Kilbourne Hole, and that also fits the data of Klaver et al. (2020), can be modelled by simple 2 component mixing (Fig. 9a, Table 5) between a peridotite-like component ($\delta^{60/58}$Ni = +0.26‰, [Ni] = 1950 ppm, [Fe] = 5.2 wt%, [Si] = 20.6 wt%) and a Fe-rich pyroxenite-like component ($\delta^{60/58}$Ni = −0.20‰, [Ni] = 450 ppm, [Fe] = 7.0 wt%, [Si] = 21.5 wt%). The $\delta^{60/58}$Ni of the pyroxenite-like component is not well constrained by the available data array, since it curves asymptotically towards that endmember. The model can also recreate the curved trend between $\delta^{60/58}$Ni and Si/Fe in this work (Fig. 9b). The model suggests that the

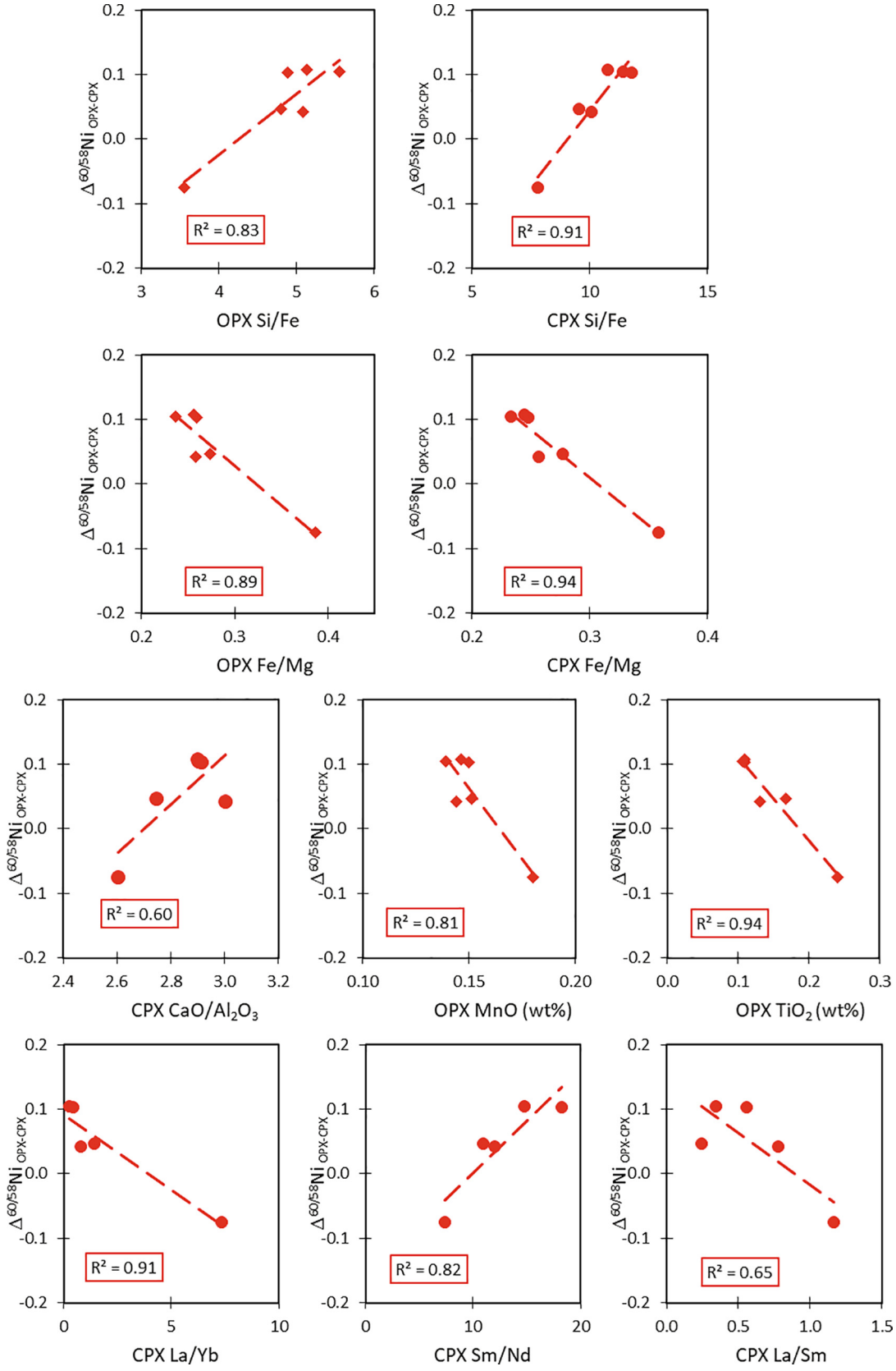

Fig. 5. $\delta^{60/58}$Ni fractionation between orthopyroxene and clinopyroxene ($\Delta^{60/58}Ni_{cpx\text{-}opx}$) and various compositional elements and ratios of the mineral phases. Kilbourne Hole elemental data from Harvey et al. (2012), Cameroon elemental data from Lee (1994).

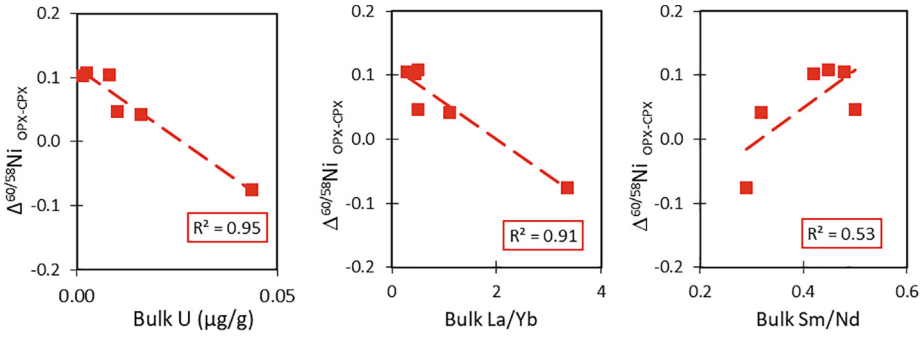

Fig. 6. $\delta^{60/58}$Ni fractionation between orthopyroxene and clinopyroxene ($\Delta^{60/58}Ni_{cpx\text{-}opx}$) and various bulk rock compositional elements and ratios. Kilbourne Hole elemental data from Harvey et al. (2012), Cameroon elemental data recalculated from mineral compositions and abundance data from Lee (1994).

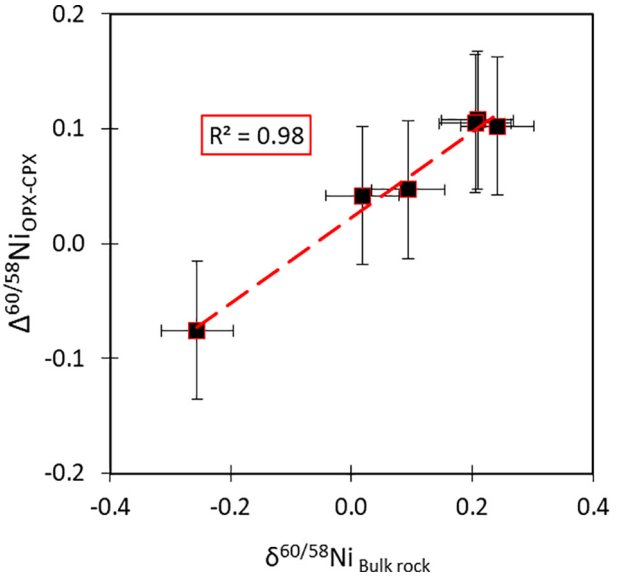

Fig. 7. $\delta^{60/58}$Ni of bulk xenoliths against the fractionation between the $\delta^{60/58}$Ni of orthopyroxene and clinopyroxene ($\Delta^{60/58}Ni_{cpx\text{-}opx}$). There is a strong positive correlation ($R^2 = 0.98$). External reproducibility of the Ni isotopic compositions is ±0.06‰.

$\delta^{60/58}$Ni of the ultramafic xenoliths from Kilbourne Hole (this work), and Horoman, Tariat and Vitim (Klaver et al., 2020) can be reproduced with between 0% and 85% Fe-rich pyroxenite-like endmember. The Kilbourne Hole pyroxenites fall at the highest contribution of the latter, as would be expected. The $\delta^{60/58}$Ni, [Fe], and [Si] in Cameroon Line websterites and Tanzanian dunites (Fig. 8d), cannot be reproduced by this mixing model indicating additional components and/or processes need to be considered in order to explain the diversity of mantle $\delta^{60/58}$Ni variation.

The relationship between bulk rock $\delta^{60/58}$Ni and iron is significant in two ways.

- A correlation between $\delta^{60/58}$Ni and Fe content, a major element, implies that Ni isotope variations are caused by a significant process that defines the bulk composition of mantle lithologies. Furthermore, the relationship with $\delta^{60/58}$Ni and Fe content is present globally, and is not part of a localised process. As the samples identified in Klaver et al. (2020) as metasomatised are similarly part of the same trend (Fig. 8c, Fig. A10), as with the metasomatised samples in this work. Therefore, metasomatic effects are not the cause of the isotopic variations.
- Major element variability in Hawaiian lavas, including Fe content, has been proposed as a key feature of identifying the proportion of pyroxenitic material in the volcanic source (Hauri, 1996). This material has been suggested to relate to recycling of oceanic crust (Hauri, 1996). Based on the Ni concentrations in melt inclusions, this reservoir may contribute a significant proportion of Ni in Hawaiian olivines and melts (Sobolev et al., 2005). Should pyroxenitic material have a light $\delta^{60/58}$Ni composition, mixing between it and more typical mantle materials with heavier $\delta^{60/58}$Ni would couple increasingly light Ni isotopic compositions with Fe enrichment. Alternatively, in-situ pyroxenite formation at Hawaii due to replacement of olivine with pyroxene by percolation of eclogite melt, as proposed by Sobolev et al. (e.g. 2005), could also affect the bulk $\delta^{60/58}$Ni if the eclogite melt should have light $\delta^{60/58}$Ni, thereby also producing heterogeneity in the mantle by mixing. The low Ni content of such eclogite melt would potentially require a more extreme Ni isotopic composition.

Magmas produced from subducted oceanic crust are enriched in light REE and other incompatible elements, and have long been thought to react with the mantle and produce olivine pyroxenites at subduction zones (e.g. Wyllie, 1982). Such Fe-rich potentially pyroxenitic material might have isotopically light Ni if melts derived from subducted oceanic crust have isotopically light Ni, or if other slab derived materials or subduction zone processes (e.g. dehydration) lead to the incorporation of light $\delta^{60/58}$Ni in the mantle. At present only limited data are available for potential subduction zone materials and processes. Data for some MORB (−0.22‰ to +0.04‰; Gall, 2011), altered ocean floor dykes (+0.00‰ to +0.14‰; Gall, 2011), and some sediments (Pre-Devonian black shales, majority $\delta^{60/58}$Ni between −0.84‰ and +0.10‰, Pašava et al., 2019), suggest that there may be direct contributions of light $\delta^{60/58}$Ni to subduction zones.

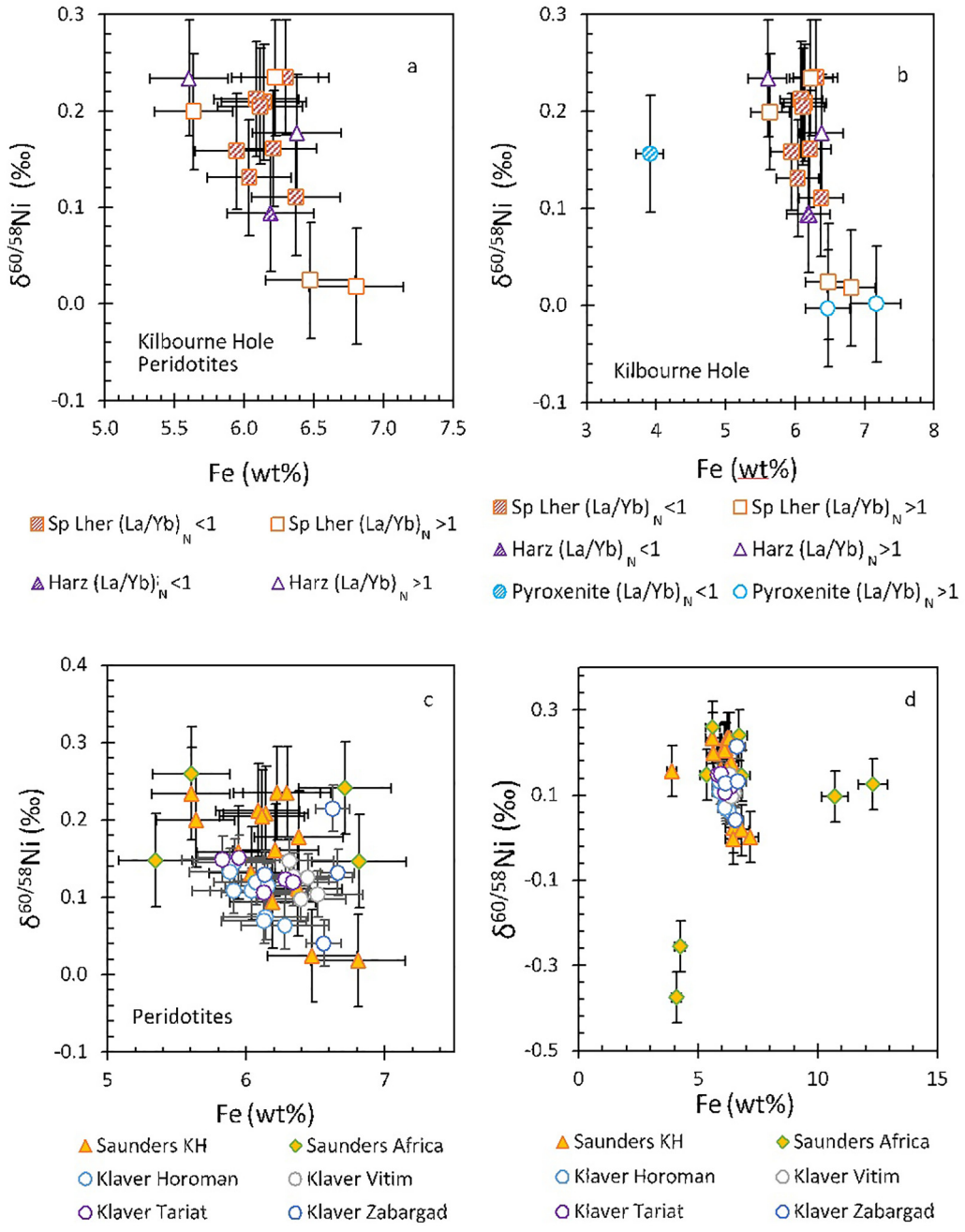

Fig. 8. (a) $\delta^{60/58}$Ni of bulk rock Kilbourne Hole peridotites against the bulk rock Fe content (wt%) from (Harvey et al., 2012). Samples are separated into lithologies (Sp Lher = spinel lherzolite, Harz = harzburgite) and whether the $(La/Yb)_N$ was > 1 (open) or < 1 (hashed). There is a negative covariation: R^2 value = 0.40, p value = 0.01. Error on Fe estimated as 5% total result. External reproducibility of the Ni isotopic compositions is ±0.06‰, presented as x-axis error bars. (b) Addition of Kilbourne Hole pyroxenites to this plot shows one depleted pyroxenite lying off trend and the other samples contributing to an improvement to statistical significance (R^2 value = 0.53, p value = 0.001, n = 17). (c) Plot of $\delta^{60/58}$Ni of bulk rock peridotites (diamonds, triangles = this work; circles = Klaver et al., 2020) against the bulk rock Fe (wt%). Fe calculated from Fe_2O_3 (Harvey et al., 2012), or FeO (Rhodes and Dawson, 1975; Takazawa et al., 2000; Brooker et al., 2004; Ionov et al., 2005; Carlson and Ionov, 2019). Samples are separated into localities, with KH = Kilbourne Hole. There is an overall negative covariation: R^2 value = 0.18, p value = 0.005. Error on Fe estimated as 5% total result. External reproducibility of the Ni isotopic compositions is ±0.06‰ (this work) and ±0.03‰ (Klaver et al., 2020), presented as x-axis error bars. For clarity plots with Klaver et al (2020) data are separated into individual plots in Fig. A10. (d) Addition of other lithologies (dunites and websterites) show that although peridotites and some pyroxenites show a global trend, there is further heterogeneity that this relationship cannot explain. Fe for Cameroon websterites calculated from published modal mineralogy proportions and Fe_2O_3 and FeO for major mineral phases (Lee, 1994), for Tanzanian dunites Fe was calculated from Fe_2O_3 and FeO: BD806 (Dawson et al., 1970) and BD825 (Rhodes and Dawson, 1975).

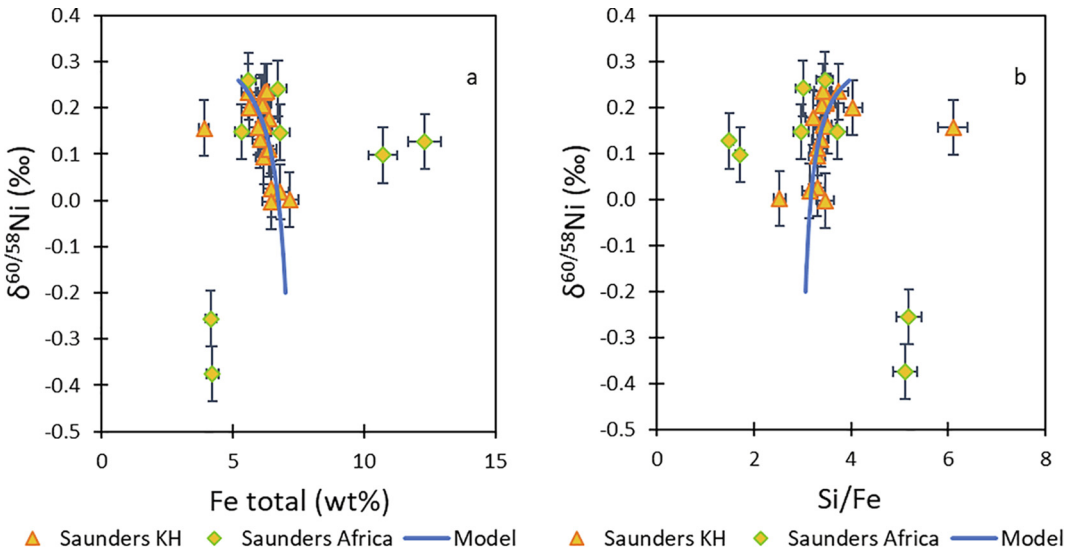

Fig. 9. $\delta^{60/58}$Ni of bulk rock compositions for xenoliths in this work (KH = Kilbourne Hole, Africa = Tanzania and Cameroon), and the 2 endmember model designed to fit the data, against Fe content (a) and Si/Fe ratio (b). Error bars on points are external reproducibility on $\delta^{60/58}$Ni of ±0.06‰ and ±5% on Fe. Fe content references as in Fig. 8, Si references in Table A1.

Table 5
Model endmember compositions.

	$\delta^{60/58}$Ni (‰)	[Ni] (μg g^{-1})	SiO_2 (wt%)	Fe (wt%)	
1	+0.26	1950	44	5.2	Mantle-like
2	−0.20	450	46	7	Fertile, enriched pyroxenite-like

Bulk rock $\delta^{60/58}$Ni in Kilbourne Hole xenoliths additionally co-varies with $^{143}Nd/^{144}Nd$ (Fig. 10, presented as εNd), including peridotites and pyroxenites. Again, the samples form a continuum, suggesting a mixing trend. Lower $^{143}Nd/^{144}Nd$ results from time-integrated enrichment in Nd/Sm (i.e. LREE enrichment; e.g. Haase et al., 2011), possibly facilitated by melt percolation as previously observed in Kilbourne Hole xenoliths (Roden et al., 1988; Harvey et al., 2012), and which could be potentially related to subduction.

5.3. The bulk silicate Earth

The published $\delta^{60/58}$Ni data for peridotite xenoliths ranges from −0.08‰ to +0.32‰ (Ratié et al., 2015; Gall et al., 2017; Spivak-Birndorf et al., 2018; Klaver et al., 2020), with additional peridotites from this work falling within this range. The peridotite $\delta^{60/58}$Ni range is only fractionally wider than the range of published data for carbonaceous chondrites +0.02‰ to +0.31‰ (Cameron et al., 2009; Steele et al., 2012; Gall et al., 2017; Klaver et al., 2020). However, $\delta^{60/58}$Ni estimates of BSE have been generally more consistent than data for carbonaceous chondrites. Two previously published estimates for Ni isotopic composition of the BSE are indistinguishable from each other at the 2σ level; ($\delta^{60/58}$Ni = +0.18±0.04‰; Steele et al. (2011), and +0.23±0.06‰; Gall et al. (2017)), while two further estimates are significantly lighter and also in complete agreement: + 0.11±0.01‰, (Elliott and Steele (2017), from the data of Gueguen et al. (2013)) and +0.12±0.05‰ (Klaver et al., 2020).

The Kilbourne Hole, Cameroon Line and Tanzanian xenoliths analysed in this work can further contribute to the elucidation of the Ni isotopic composition of the BSE. These xenoliths expand the geographical range as well as lithological variety and number of individual samples available for BSE estimates. Literature BSE estimates exclude samples showing evidence of metasomatism, however, this work provides evidence that metasomatism is not the dominant process for producing $\delta^{60/58}$Ni heterogeneity. Additionally, the unmetasomatised fertile peridotites from this work, averaging $\delta^{60/58}$Ni = +0.19±0.09‰ (2SD, n = 18), overlap with the analytical uncertainty of the average $\delta^{60/58}$Ni of metasomatised peridotites from this work, +0.11±0.15‰ (2SD, n = 6). These averages are all within analytical uncertainty of published BSE estimates.

To improve on current BSE estimates it would be necessary to derive a clearer understanding of the origins of the observed heterogeneity in $\delta^{60/58}$Ni and the volumetric importance of associated materials. The heterogeneity observed in peridotites in this work, combined with published data (Gall et al., 2017; Klaver et al., 2020) provides further evidence that widespread heterogeneity in $\delta^{60/58}$Ni is ubiquitous in the terrestrial mantle, and should be accounted for in BSE estimates. The range of $\delta^{60/58}$Ni in the pyroxenites (−0.38‰ to +0.16‰) expands mantle heterogeneity to isotopically lighter $\delta^{60/58}$Ni than previously reported. Further, given the lack of isotopic fraction-

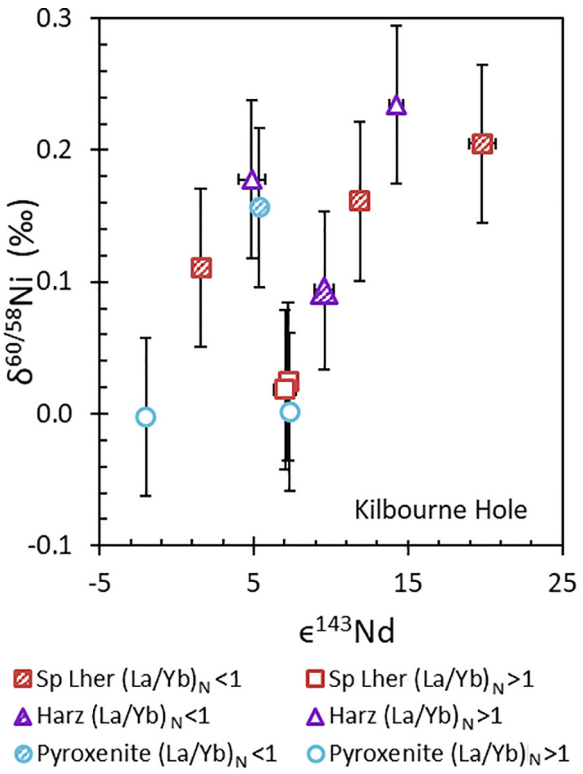

Fig. 10. $\delta^{60/58}$Ni of bulk rock Kilbourne Hole xenoliths and the bulk rock isotopic $^{143}Nd/^{144}Nd$ composition, where available. Neodymium data from (Harvey et al., 2012) and presented in Table A1. Samples are separated into lithologies and whether the $(La/Yb)_N$ (chondrite normalised ratio of Light REE La to Heavy REE Yb was >1 or <1 indicating Light REE enrichment or depletion relative to chondrites). ϵ^{143}Nd obtained using a value $^{143}Nd/^{144}Nd = 0.512638$ for BSE (Bouvier et al., 2008), where Nd isotopic composition available. The trend improves to R^2 value = 0.36, p value = 0.05. External reproducibility of the Ni isotopic compositions is ±0.06‰, presented as x-axis error bars, Nd error bars from Harvey et al. (2012).

ation associated with melting, the range of $\delta^{60/58}$Ni in MORB (−0.22‰ to +0.24‰, Cameron et al., 2009; Gall, 2011) provides additional evidence of isotopically light Ni variations in the mantle. Therefore, the best estimate of the current mantle and BSE may not be reliably represented by an average for unmetasomatised peridotite.

6. CONCLUSIONS

1. The mantle is heterogeneous in $\delta^{60/58}$Ni. Isotopic heterogeneity for an element with such a high concentration in the mantle, and no changes in redox state in mantle conditions is surprising.
2. The $\delta^{60/58}$Ni of unmetasomatised fertile mantle based on spinel lherzolites and harzburgites is 019±0.09‰, within analytical uncertainty of the comparable published averages. Further work is needed to understand to what extent it represents the BSE, given the existence of lighter $\delta^{60/58}$Ni in some samples.
3. There is no evidence that metasomatism has is a dominant control Ni isotopic compositions in bulk ultramafic rocks.
4. On crystallisation, minerals preserve the $\delta^{60/58}$Ni of the ambient mantle with negligible inter-mineral fractionation, limited to <0.12‰.
5. $\Delta^{60/58}Ni_{cpx\text{-}opx}$ varies with mineral chemistry (including Si/Fe and Fe/Mg of orthopyroxene and clinopyroxene, clinopyroxene La/Yb, Sm/Nd, La/Sm, and orthopyroxene TiO_2). Further, $\Delta^{60/58}Ni_{cpx\text{-}opx}$ has a strong relationship with bulk rock $\delta^{60/58}$Ni, and [U], and other ratios observed to correlate in individual mineral compositions. These relationships imply that mineral Ni isotopic compositions are related to features associated with enrichment and fertility.
6. Inter-mineral $\delta^{60/58}$Ni differences are too small to account for Ni isotope variation in the mantle.
7. The isotopic composition of constituent minerals can be used to reconstruct the bulk $\delta^{60/58}$Ni, showing that minor phases and interstitial alteration products do not influence the bulk $\delta^{60/58}$Ni of mantle rocks. Garnet and sulphide cannot contribute significantly to the bulk rock Ni budgets of mantle rocks.
8. Correlations between $\delta^{60/58}$Ni and $^{143}Nd/^{144}Nd$ and iron concentration in bulk ultramafic xenoliths from Kilbourne Hole provide evidence for the association of light $\delta^{60/58}$Ni with enriched mantle lithologies. The correlation with iron is also observed in literature data (Klaver et al., 2020). Ancient recycling of subducted residual oceanic crust is a likely mechanism for producing such enriched lithologies and hence Ni isotope variability in the mantle.

Declaration of Competing Interest

The authors declare that they have no known competing financial interests or personal relationships that could have appeared to influence the work reported in this paper.

ACKNOWLEDGMENTS

This work was supported by an STFC PhD studentship (1508639) awarded to NJS from with additional funding from STFC Planetary Origins and Developments grant: ST/M001318/1 awarded to ANH, and from the Universities of Oxford and Columbia, and NERC award NE/J017981/1 to JH. MC-ICPMS analyses were aided by Yu-Te Alan Hsieh; ICPMS analyses by Philip Holdship. Samples from Africa were from the collections of the late Barry Dawson, the PhD work of Cassi Paslick and Der-Chuen Lee, and the collection of ANH. Sally Gibson, University of Cambridge, supplied further information, and thin sections, left in her care by Barry Dawson. We thank Shichun Huang, Jian Huang, and an anonymous reviewer for extremely constructive comments.

APPENDIX A. SUPPLEMENTARY MATERIAL

Supplementary data to this article can be found online at https://doi.org/10.1016/j.gca.2020.06.029.

REFERENCES

Atouba L. C. O., Chazot G., Moundi A., Agranier A., Bellon H., Nonnotte P., Nzenti J. P. and Kankeu B. (2016) Mantle sources

beneath the Cameroon Volcanic Line: geochemistry and geochronology of the Bamoun plateau mafic rocks. *Arab. J. Geosci.*, 9.

Archer C., Vance D., Milne A. and Lohan M. C. (2020) The oceanic biogeochemistry of nickel and its isotopes: New data from the South Atlantic and the Southern Ocean biogeochemical divide. *Earth Planet. Sci. Lett.* **535** 116118.

Bouvier A., Vervoort J. D. and Patchett P. J. (2008) The Lu-Hf and Sm-Nd isotopic composition of CHUR: constraints from unequilibrated chondrites and implications for the bulk composition of terrestrial planets. *Earth Planet. Sci. Lett.* **273**, 48–57.

Brey G. P. and Köhler T. (1990) Geothermobarometry in four-phase lherzolites II. New thermobarometers, and practical assessment of existing thermobarometers. *J. Petrol.* **31**, 1353–1378. https://doi.org/10.1093/petrology/31.6.1353.

Brey G. P., Köhler T. and Nickel K. G. (1990) Geothermobarometry in four-phase lherzolites I. experimental results from 10 to 60 kb. *J. Petrol.* **31**, 1313–1352.

Brooker R. A., James R. H. and Blundy J. D. (2004) Trace elements and Li isotope systematics in Zabargad peridotites: Evidence of ancient subduction processes in the Red Sea mantle. *Chem. Geol.* **212**, 179–204.

Burns R. G. (1970) Site preferences of transition metal ions in silicate crystal structures. *Chem. Geol.* **5**, 275–283.

Burton K. W., Schiano P., Birck J.-L., Allègre C. J., Rehkämper M., Halliday A. N. and Dawson J. B. (2000) The distribution and behaviour of rhenium and osmium amongst mantle minerals and the age of the lithospheric mantle beneath Tanzania. *Earth Planet. Sci. Lett.* **183**, 93–106. https://doi.org/10.1016/S0012-821X(00)00259-4.

Cameron V. and Vance D. (2014) Heavy nickel isotope compositions in rivers and the oceans. *Geochim. Cosmochim. Acta* **128**, 195–211. https://doi.org/10.1016/j.gca.2013.12.007.

Cameron V., Vance D., Archer C. and House C. H. (2009) A biomarker based on the stable isotopes of nickel. *Proc. Natl. Acad. Sci.* **106**, 10944–10948.

Carlson R. W. and Ionov D. A. (2019) Compositional characteristics of the MORB mantle and bulk silicate earth based on spinel peridotites from the Tariat Region, Mongolia. *Geochim. Cosmochim. Acta* **257**, 206–223.

Chako Tchamabe T. B., Youmen D., Owona S., Issa O. T., Németh K., Ngapna M. N., Asaah A. N. E., Aka F. T., Tanyileke G. and Hell J. V. (2013) Eruptive history of the Barombi Mbo Maar, Cameroon volcanic line, Central Africa: constraints from volcanic facies analysis. *Cent. Eur. J. Geosci.* **5**, 480–496.

Chernonozhkin S. M., Goderis S., Lobo L., Claeys P. and Vanhaecke F. (2015) Development of an isolation procedure and MC-ICP-MS measurement protocol for the study of stable isotope ratio variations of nickel. *J. Anal. At. Spectrom.* **30**, 1518–1530. https://doi.org/10.1039/C5JA00080G.

Ciscato E. R., Bontognali T. R. R. and Vance D. (2018) Nickel and its isotopes in organic-rich sediments: implications for oceanic budgets and a potential record of ancient seawater. *Earth Planet. Sci. Lett.* **494**, 239–250. https://doi.org/10.1016/j.epsl.2018.04.061.

Cohen R. S., O'Nions R. K. and Dawson J. B. (1984) Isotope geochemistry of xenoliths from East Africa: Implications for development of mantle reservoirs and their interaction. *Earth Planet. Sci. Lett.* **68**, 209–220 https://www.sciencedirect.com/science/article/pii/0012821X84901535.

Dawson J. B. (1999) Melting and metasomatism in upper mantle peridotite xenoliths from Labait, North-central Tanzania, and contrasting metasomatic styles in the Tanzanian lithospheric mantle. In *Proceedings of the 7th International Kimberlite Conference*, pp. 1987–1988.

Dawson J. B. (2002) Metasomatism and partial melting in upper-mantle peridotite xenoliths from the Lashaine Volcano, Northern Tanzania. *J. Petrol.* **43**, 1749–1777.

Dawson J. B. (2012) Nephelinite–melilitite–carbonatite relationships: evidence from Pleistocene–recent volcanism in northern Tanzania. *Lithos* **152**, 3–10. https://doi.org/10.1016/j.lithos.2012.01.008.

Dawson J. B., Powell D. G. and Reid A. M. (1970) Ultrabasic xenoliths and lava from the Lashaine. *J. Petrol.* **11**, 519–548.

Dawson J. B. and Smith J. V. (1973) Alkalic pyroxenite xenoliths from the Lashaine volcano, Northern Tanzania. *J. Petrol.* **14**, 113–131.

Deer W. A., Howie R. A. and Zussman J. (1966) An Introduction to Rock Forming Minerals, first ed.

Elliott T. and Steele R. C. J. (2017) The isotope geochemistry of Ni. *Rev. Mineral. Geochem.*.

Estrade N., Cloquet C., Echevarria G., Sterckeman T., Deng T., Tang YeTa and Morel J.-L. (2015) Weathering and vegetation controls on nickel isotope fractionation in surface ultramafic environments (Albania). *Earth Planet. Sci. Lett.* **423**, 24–35. https://doi.org/10.1016/j.epsl.2015.04.018.

Fitton J. G. (1987) The Cameroon line, West Africa: a comparison between oceanic and continental alkaline volcanism. In *Alkaline Igneous Rocks, Geological Society Special Publications No. 30*, pp. 273–291.

Fitton J. G. and Dunlop H. M. (1985) The Cameroon line, West Africa, and its bearing on the origin of oceanic and continental alkali basalt. *Earth Planet. Sci. Lett.* **72**, 23–38. https://doi.org/10.1016/0012-821X(85)90114-1.

France L., Chazot G., Kornprobst J., Dallai L., Vannucci R., Grégoire M., Bertrand H. and Boivin P. (2015) Mantle refertilization and magmatism in old orogenic regions: the role of late-orogenic pyroxenites. *Lithos* **232**, 49–75.

Gall L. (2011) Development and Application of Nickel Stable Isotopes as a New Geochemical Tracer. Ph.D. thesis, Univ. of Oxford.

Gall L., Williams H. M., Halliday A. N. and Kerr A. C. (2017) Nickel isotopic composition of the mantle. *Geochim. Cosmochim. Acta* **199**, 196–209. https://doi.org/10.1016/j.gca.2016.11.016.

Gall L., Williams H. M., Siebert C., Halliday A. N., Herrington R. J. and Hein J. R. (2013) Nickel isotopic compositions of ferromanganese crusts and the constancy of deep ocean inputs and continental weathering effects over the Cenozoic. *Earth Planet. Sci. Lett.* **375**, 148–155. https://doi.org/10.1016/j.epsl.2013.05.019.

Gall L., Williams H., Siebert C. and Halliday A. N. (2012) Determination of mass-dependent variations in nickel isotope compositions using double spiking and MC-ICPMS. *J. Anal. At. Spectrom.* **27**, 137–145.

Gibson S. A., McMahon S. C., Day J. A. and Dawson J. B. (2013) Highly refractory lithospheric mantle beneath the Tanzanian craton: evidence from Lashaine pre-metasomatic garnet-bearing peridotites. *J. Petrol.* **54**, 1503–1546.

Gramlich J. W., Machlan L. A., Barnes I. L. and Paulsen P. J. (2012) Absolute isotopic abundance ratios and atomic weight of a reference sample of nickel. *J. Res. Natl. Inst. Stand. Technol.* **94**, 347.

Gueguen B., Rouxel O., Ponzevera E., Bekker A. and Fouquet Y. (2013) Nickel isotope variations in terrestrial silicate rocks and geological reference materials measured by MC-ICP-MS. *Geostand. Geoanalyt. Res.* **37**, 297–317.

Gueguen B., Rouxel O., Rouget M.-L., Bollinger C., Ponzevera E., Germain Y. and Fouquet Y. (2016) Comparative geochemistry of four ferromanganese crusts from the Pacific Ocean and significance for the use of Ni isotopes as paleoceanographic tracers. *Geochim. Cosmochim. Acta* **189**, 214–235. https://doi.org/10.1016/j.gca.2016.06.005.

Haase K. M., Regelous M., Duncan R. A., Brandl P. A., Stroncik N. and Grevemeyer I. (2011) Insights into mantle composition and mantle melting beneath mid-ocean ridges from postspreading volcanism on the fossil Galapagos Rise. *Geochem. Geophys. Geosy.* **12**.

Halliday A. N., Dickin A. P., Fallick A. E. and Fitton J. G. (1988) Mantle dynamics: A Nd, Sr, Pb and O isotopic study of the Cameroon line volcanic chain. *J. Petrol.* **29**, 181–211.

Harvey J., Dale C. W., Gannoun A. and Burton K. W. (2011) Osmium mass balance in peridotite and the effects of mantle-derived sulphides on basalt petrogenesis. *Geochim. Cosmochim. Acta* **75** (19), 5574–5596. https://doi.org/10.1016/j.gca.2011.07.001.

Harvey J., König S. and Luguet A. (2015) The effects of melt depletion and metasomatism on highly siderophile and strongly chalcophile elements: S-Se-Te-Re-PGE systematics of peridotite xenoliths from Kilbourne Hole, New Mexico. *Geochim. Cosmochim. Acta* **166**, 210–233.

Harvey J., Yoshikawa M., Hammond S. J. and Burton K. W. (2012) Deciphering the trace element characteristics in Kilbourne Hole peridotite xenoliths: Melt-rock interaction and metasomatism beneath the Rio Grande Rift, SW USA. *J. Petrol.* **53**, 1709–1742.

Hauri E. H. (1996) Major-element variability in the Hawaiian mantle plume. *Nature* **386**.

Hellebrand E., Snow J. E., Dick H. J. B. and Hofmann A. W. (2001) Coupled major and trace elements as indicators of the extent of melting in mid-ocean-ridge peridotites. *Nature* **410**, 677–681 http://www.nature.com/articles/35070546.

Hofmann A., Bekker A., Dirks P., Gueguen B., Rumble D. and Rouxel O. J. (2014) Comparing orthomagmatic and hydrothermal mineralization models for komatiite-hosted nickel deposits in Zimbabwe using multiple-sulfur, iron, and nickel isotope data. *Miner. Depos.* **49**, 75–100.

Ionov D. A., Ashchepkov I. and Jagoutz E. (2005) The provenance of fertile off-craton lithospheric mantle: Sr-Nd isotope and chemical composition of garnet and spinel peridotite xenoliths from Vitim, Siberia. *Chem. Geol.* **217**, 41–75.

Irving A. (1980) Petrology and geochemistry of composite ultramafic xenoliths in alkalic basalts and implications for magmatic processes within the mantle. *Am. J. Sci.* **280-A**, 389–426.

Kamgang P., Chazot G., Njonfang E., Ngongang N. B. T. and Tchoua F. M. (2013) Mantle sources and magma evolution beneath the Cameroon Volcanic Line: geochemistry of mafic rocks from the Bamenda Mountains (NW Cameroon). *Gondwana Res.* **24**, 727–741.

Kil Y. and Wendlandt R. F. (2007) Depleted and enriched mantle processes under the Rio Grande rift: spinel peridotite xenoliths. *Contrib. Mineral. Petrol.* **154**, 135–151 http://link.springer.com/10.1007/s00410-007-0183-y.

Klaver M., Ionov D. A., Takazawa E. and Elliott T. (2020) The non-chondritic Ni isotope composition of Earth's mantle. *Geochim. Cosmochim. Acta* **268**, 405–421.

König S., Wille M., Voegelin A. and Schoenberg R. (2016) Molybdenum isotope systematics in subduction zones. *Earth Planet. Sci. Lett.* **447**, 95–102.

Koornneef J. M., Davies G. R., Döpp S. P., Vukmanovic Z., Nikogosian I. K. and Mason P. R. D. (2009) Nature and timing of multiple metasomatic events in the sub-cratonic lithosphere beneath Labait, Tanzania. *Lithos* **112**, 896–912. https://doi.org/10.1016/j.lithos.2009.04.039.

Lee C.-T. and Rudnick R. (1999a) The origin and demise of cratonic lithosphere: a geochemical perspective from the Tanzanian craton. In *Proceedings of the 7th International Kimberlite Conference*, pp. 492–494.

Lee C.-T. and Rudnick R. L. (1999b) Compositionally stratified cratonic lithosphere and geochemistry of peridototic xenoliths from the Labait volcano Tanzania. In Proceedings of the 7th International Kimberlite Conference, pp. 503–521. https://www.researchgate.net/publication/290162967.

Lee D.-C. (1994) A Chemical, Isotopic, and Geochronological Study of the Cameroon Line, West Africa. Ph.D. thesis, Univ. of Michigan.

Lee D.-C., Halliday A. N., Davies G. R., Essene E. J., Fitton J. G. and Temdjim R. (1996) Melt enrichment of shallow depleted mantle: a detailed petrological, trace element and isotopic study of mantle-derived xenoliths and megacrysts from the Cameroon line. *J. Petrol.* **37**, 415–441.

Lee D.-C., Halliday A. N., Fitton J. G. and Poli G. (1994) Isotopic variations with distance and time in the volcanic islands of the Cameroon line: evidence for a mantle plume origin. *Earth Planet. Sci. Lett.* **123**, 119–138.

Lorand J. P. (1990) Are spinel Iherzolite xenoliths representative of the abundance of sulfur in the upper mantle? *Geochim. Cosmochim. Acta* **54**, 1487–1492 https://www.sciencedirect.com/science/article/pii/001670379090173I.

Marzoli A., Renne P. R., Piccirillo E. M., Francesca C., Melfi A. J., Nyobe J. B. and N'ni J. (1999) Silicic magmas from the continental Cameroon Volcanic Line (Oku, Bambouto, Ngaoundere): ^{40}Ar-^{39}Ar dates, petrology, Sr-Nd-O isotopes and their petrogenetic significance. *Contrib. Mineral. Petrol.* **135**, 133–150.

McDonough W. F. and Sun S.-s. (1995) The composition of the Earth. *Chem. Geol.* **120**, 223–253. https://doi.org/10.1016/0009-2541(94)00140-4.

Nicholls D. (1974) Complexes and First Row Transition Elements. Macmillan, London.

O'Neill H. S. (1991) The origin of the moon and the early history of the earth—A chemical model. Part 2: The earth. *Geochim. Cosmochim. Acta* **55**, 1159–1172 https://www.sciencedirect.com/science/article/pii/0016703791901696.

Palme H. and O'Neill H. S. C. (2007) Cosmochemical estimates of mantle composition. *Treatise Geochem.*, 1–38 https://www.sciencedirect.com/science/article/pii/B0080437516021770?via%3Dihub.

Pašava J., Chrastný V., Loukola-Ruskeeniemi K. and Šebek O. (2019) Nickel isotopic variation in black shales from Bohemia, China, Canada, and Finland: a reconnaissance study. *Miner. Depos.* **54**, 719–742 http://link.springer.com/10.1007/s00126-018-0839-8.

Paslick C. R. (1995) A Geochemical Study of Volcanism Associated with the Early Stages of Continental Rifting in Northern Tanzania, Ph.D. thesis, Univ. of Michigan.

Perkins D. and Anthony E. Y. (2011) The evolution of spinel lherzolite xenoliths and the nature of the mantle at Kilbourne Hole, New Mexico. *Contrib. Mineral. Petrol.* **162**, 1139–1157 http://link.springer.com/10.1007/s00410-011-0644-1.

Pike J. E. N., Meyer C. E. and Wilshire H. G. (1980) Petrography and chemical composition of a suite of ultramafic xenoliths from Lashaine, Tanzania. *J. Geol.* **88**, 343–352.

Pintér Z., Tene Djoukam J. F., Mihály J., Jeffries T., Falus G., Németh C., Tchouankoue J. P., Konc Z., Barou F., Patkó L., Kovács I. and Tommasi A. (2015) Characterization of the subcontinental lithospheric mantle beneath the Cameroon volcanic line inferred from alkaline basalt hosted peridotite xenoliths from Barombi Mbo and Nyos Lakes. *J. African Earth Sci.* **111**, 170–193.

Porter S. J., Selby D. and Cameron V. (2014) Characterising the nickel isotopic composition of organic-rich marine sediments. *Chem. Geol.* **387**, 12–21. https://doi.org/10.1016/j.chemgeo.2014.07.017.

Putirka K., Ryerson F. J., Perfit M. and Ridley W. I. (2011) Mineralogy and composition of the oceanic mantle. *J. Petrol.* **52**, 279–313.

Ratié G., Jouvin D., Garnier J., Rouxel O., Miska S., Guimarães E., Cruz Vieira L., Sivry Y., Zelano I., Montarges-Pelletier E., Thil F. and Quantin C. (2015) Nickel isotope fractionation during tropical weathering of ultramafic rocks. *Chem. Geol.* **402**, 68–76. https://doi.org/10.1016/j.chemgeo.2015.02.039.

Ratié G., Quantin C., Jouvin D., Calmels D., Ettler V., Sivry Y., Vieira L. C., Ponzevera E. and Garnier J. (2016) Nickel isotope fractionation during laterite Ni ore smelting and refining: Implications for tracing the sources of Ni in smelter-affected soils. *Appl. Geochem.* **64**, 136–145.

Ratié G., Quantin C., Maia De Freitas A., Echevarria G., Ponzevera E. and Garnier J. (2019) The behavior of nickel isotopes at the biogeochemical interface between ultramafic soils and Ni accumulator species. *J. Geochem. Explor.* **196**, 182–191 https://www.sciencedirect.com/science/article/pii/S0375674218302395.

Reid A. M. and Dawson J. B. (1972) Olivine-garnet reaction in peridotites from Tanzania. *Lithos* **5**, 115–124 https://www.sciencedirect.com/science/article/pii/0024493772900631.

Reid A. M., Donaldson C. H., Brown R. W., Ridley W. I. and Dawson J. B. (1975) Mineral chemistry of peridotite xenoliths from the Lashaine volcano, Tanzania. *Phys. Chem. Earth* **9**, 525–543.

Rhodes J. M. and Dawson J. B. (1975) Major and trace element chemistry of garnet and spinel peridotites from the Lashaine Volcano, Tanzania. *Phys. Chem. Earth* **37**.

Ridley W. I. and Dawson J. B. (1975) Lithophile trace element data bearing on the origin of peridotite xenoliths, ankaramite and carbonatite from Lashaine volcano, N. Tanzania. *Phys. Chem. Earth* **9**, 559–569.

Roden M. F., Irving A. J. and Murthy V. R. (1988) Isotopic and trace element composition of the upper mantle beneath a young continental rift: Results from Kilbourne Hole, New Mexico. *Geochim. Cosmochim. Acta* **52**, 461–473.

Satsukawa T., Michibayashi K., Anthony E. Y., Stern R. J., Gao S. S. and Liu K. H. (2011) Seismic anisotropy of the uppermost mantle beneath the Rio Grande rift: Evidence from Kilbourne Hole peridotite xenoliths, New Mexico. *Earth Planet. Sci. Lett.* **311**, 172–181. https://doi.org/10.1016/j.epsl.2011.09.013.

Shannon R. D. (1976) Revised Effective Ionic Radii and Systematic Studies of Interatomic Distances in Halides and Chalcogenides.

Shaw D. M. (1979) Trace element melting models. *Phys. Chem. Earth.* **11**, 577–586 https://www.sciencedirect.com/science/article/pii/0079194679900557.

Siebert C., Nägler T. F. and Kramers J. D. (2001) Determination of molybdenum isotope fractionation by double-spike multicollector inductively coupled plasma mass spectrometry. *Geochem. Geophys. Geosy.* **2**.

Sobolev A. V., Hofmann A. W., Sobolev S. V. and Nikogosian I. K. (2005) An olivine-free mantle source of Hawaiian shield basalts. *Nature* **434**, 590–597. https://doi.org/10.1038/nature03411.

Sossi P. A., Foden J. D. and Halverson G. P. (2012) Redox-controlled iron isotope fractionation during magmatic differentiation: An example from the Red Hill intrusion. *S. Tasmania. Contrib. Mineral. Petrol.* **164**, 757–772.

Spivak-Birndorf L. J., Wang S.-J., Bish D. L. and Wasylenki L. E. (2018) Nickel isotope fractionation during continental weathering. *Chem. Geol.* **476**, 316–326.

Steele R. C. J., Coath C. D., Regelous M., Russell S. and Elliott T. (2012) Neutron-poor nickel isotope anomalies in meteorites. *Astrophys. J.*, 758.

Steele R. C. J., Elliott T., Coath C. D. and Regelous M. (2011) Confirmation of mass-independent Ni isotopic variability in iron meteorites. *Geochim. Cosmochim. Acta* **75**, 7906–7925. https://doi.org/10.1016/j.gca.2011.08.030.

Suh C. E., Luhr J. F. and Njome M. S. (2008) Olivine-hosted glass inclusions from Scoriae erupted in 1954–2000 at Mount Cameroon volcano, West Africa. *J. Volcanol. Geotherm. Res.* **169**, 1–33.

Takazawa E., Frey F. A., Shimizu N. and Obata M. (2000) Whole rock compositional variations in an upper mantle peridotite (Horoman, Hokkaido, Japan): are they consistent with a partial melting process? *Geochim. Cosmochim Acta* **64**, 695–716.

Tanimizu M. and Hirata T. (2006) Determination of natural isotopic variation in nickel using inductively coupled plasma mass spectrometry. *J. Anal. At. Spectrom.* **21**, 1423–1426.

Tedonkenfack S. S. T., Tamen J., Nkouathio D. G., Asaah A. N. E., Gountié-Dedzoedzo M. and Aka F. T. (2019) Petrography and geochemistry of mantle xenoliths from Ibal-Oku region (North-West region, Cameroon): Preliminary evidence of mantle heterogeneities. *J. African Earth Sci.* **154**, 70–79 https://www.sciencedirect.com/science/article/pii/S1464343X19300913.

Vance D., Little S. H., Archer C., Cameron V., Andersen M. B., Rijkenberg M. J. A. and Lyons T. W. (2016) The oceanic budgets of nickel and zinc isotopes: the importance of sulfidic environments as illustrated by the Black Sea. *Philos. Trans. Royal. Soc. London, A* **374**. https://doi.org/10.1098/rsta.2015.0294.

Ventura G. T., Gall L., Siebert C., Prytulak J., Szatmari P., Hürlimann M. and Halliday A. N. (2015) The stable isotope composition of vanadium, nickel, and molybdenum in crude oils. *Appl. Geochem.* **59**, 104–117. https://doi.org/10.1016/j.apgeochem.2015.04.009.

Wang R.-M., Archer C., Bowie A. R. and Vance D. (2019) Zinc and nickel isotopes in seawater from the Indian Sector of the Southern Ocean: the impact of natural iron fertilization versus Southern Ocean hydrography and biogeochemistry. *Chem. Geol.* **511**, 452–464 https://www.sciencedirect.com/science/article/pii/S0009254118304509.

Wedepohl K. H. (1974) Nickel. *Handook of Geochemistry*.

Williams H. M., Prytulak J., Woodhead J. D., Kelley K. A., Brounce M. and Plank T. (2018) Interplay of crystal fractionation, sulfide saturation and oxygen fugacity on the iron isotope composition of arc lavas: An example from the Marianas. *Geochim. Cosmochim. Acta* **226**, 224–243. https://doi.org/10.1016/j.gca.2018.02.008.

Wilshire H. G. (1984) Mantle metasomatism: the REE story. In *Geology*, 12, p. 395. Geology https://pubs.geoscienceworld.org/geology/article/12/7/395-398/198525.

Wyllie P. J. (1982) Subduction products according to experimental prediction. *Geol. Soc. Am. Bull.* **93**, 468 https://pubs.geoscienceworld.org/gsabulletin/article/93/6/468-476/202741.

Young E. D., Galy A. and Nagahara H. (2002) Kinetic and equilibrium mass-dependent isotope fractionation laws in nature and their geochemical and cosmochemical significance. *Geochim. Cosmochim. Acta* **66**, 1095–1104.

Zhang S., Rudnick R. and McCammon C. (2018) Oxidation of lithospheric mantle beneath Tanzania by melt reaction. In *Proceedings of the 11th International Kimberlite Conference*, pp. 3–5.

Zhao X., Zhang Z., Huang S., Liu Y., Li X. and Zhang H. (2017) Coupled extremely light Ca and Fe isotopes in peridotites. *Geochim. Cosmochim. Acta* **208**, 368–380. https://doi.org/10.1016/j.gca.2017.03.024.

Associate editor: Stefan Weyer